Azine Based Oligoesteric Chemosensors for Cu^{2+} Ion Detection: Synthesis, Structural Characterization, and Theoretical Investigations

Subramani Manigandan
Chonnam National University
Athianna Muthusamy (muthusrkv@gmail.com)
Sri Ramakrishna Mission Vidyalaya College of Arts and Science
Siddeswaran Anand
K.S.R. College of Engineering, KSR Kalvinagar

Research Article

Keywords: Cu2+sensor, azine oligomers, solution polymerization, chemosensors, DFT, electrical study

Posted Date: February 19th, 2024

DOI: https://doi.org/10.21203/rs.3.rs-3945531/v1

Additional Declarations: No competing interests reported.

Abstract

Synthesized monomer and its three oligoester were characterized by technique such as ^{1}H, ^{13}C, IR,UV, GPC and applied to chemosensor applications. A series of metal ion was studied with fluorophores to evaluate the sensitivity towards Cu^{2+} ion. The fluorophores results exhibit the selective and sensitive “turn off” fluorescence response with Cu^{2+} ion in DMF/H_2O (1:1, pH: 7.4, fluorophore: 5μM) solution. Binding stoichiometry and binding constant of fluorophores were calculated using Stern-Volmer equation and Benesi–Hildebrand plots respectively. Structure of fluorophores were studied using DFT, B3LYP/6–311 + + G(d,p) level basis set. Quenching mechanism and electrical properties of fluorophores were explained with theoretical outcomes. Iodine doped and undoped oligoesters electrical conductivity were studied in solid-state and the conductivity was gradually increase with increase the contact time of iodin with oligoesters. At different frequencies and temperatures, the dielectric measurement was calculated using the two-probe method. Among all oligoesters, DMDAP exhibited high electrical conductivity and DMDMP has high dielectric constant value than other oligoesters.

1. Introduction

The first-row transition element Cu^{2+} ion is most essential metal ion in the living system which plays a important in various environmental and biological processes[1–5]. According to the Environmental Protection Agency (EPA) of U.S. the concentration of Cu up to 1.3 mg L^{-1} in drinking water are tolerable[6–8]. Cu^{2+} contain hemocyanin in insects plays as oxygen transporter and in the human body Cu^{2+} is present in several enzymes, including superoxide tyrosinase, dopamine hydroxylase and dismutase. The major concentration of Cu^{2+} found in the liver, heart, kidney and brain which is key component for many biological function. Excess concentration of Cu^{2+} ion cause DNA breakage, mitochondrial damage, Alzheimer’s neuronal injury and Wilson’s diseases. Although, the deficiency of Cu^{2+} ion causes illness such as anemia[9–13]. The concentration variation of Cu^{2+} ion can disturb nutrient absorption and transport, thus destroying plant and aquatic ecosystems[14–16]. Therefore, finding the concentration of Cu^{2+} ion in environment and biological system is an essential thing.

There are several methods are used for sensing copper ions concentration such as atomic absorption spectroscopy, inductively coupled plasma and electrochemical tools. However, they required expensive equipment, sample pretreatment, sample can spoil during the analysis process and it could not apply to living organisms for bioimaging[5, 17–19]. On the two decay, the chemosensor method received much attention because of overcome those defects[20, 21]. This method is very cheap, easy to handle and very sensitive[22, 23]. Moreover, chemosensor’s sensing method can be used to applied for real-time bioimaging of various analytes.

Low-molecular-weight conjugated oligomers have enormous benefits among the chemosensors that provide the greatest advantages for biological, amplifying, and electronic communication applications[24]. Oligomers' changes in electron density in their structure can be sensitively recognised from the influences of external structure due to their conjugated double bond in the backbone structure. Particularly, the conjugated molecule with the = N-N = and -C = N- moieties functions as an effective chemosensor and has a good ligand with a significant fluorescence response to metal cations [25–27].

Therefore, developing the chemosensors for sensing Cu^{2+} ion is essential. In our work, we synthesized azine monomer and oligoesters with different degrees of substituents for detect Cu^{2+} ion. The results of chemosensors exposes sensitive response to Cu^{2+} ion detection over the presence of other metal ion. oligoesters are subjected to electrical studies. The mechanism of fluorescence quenching, conductivity and dielectric properties of oligoesters are explained using absorption spectrum and DFT parameters analysis.

2. EXPERIMENTAL

2.1. Materials

Hydrazine hydrate, benzil, 2–hydroxy benzaldehyde, phenylphosphonic dichloride, phenyldichloro phosphate and adipoyl dichloride were purchased from Merck Chemical Co. and used without further purification. Dimethyl sulfoxide, tetrahydrofuran, dimethylformamide, ethanol, acetone, acetonitrile, methanol, ethyl acetate, n–hexane, heptane, toluene, chloroform and triethylamine were obtained from Merck, India and used after the proper distillations[28].

2.2. Synthesis of monomer

2.3. Synthesis of 2,2–(((1,2–diphenylethane–1,2–diylidene)bis(hydrazine–2,1–diylidene))bis(methanylylidene))diphenol (DBHMD)

2–(Hydrazinelidenemethyl)phenol (2BH) and benzil were separately dissolved in methanol and mixed (2:1 molar ratio) thenrefluxed for 6 hrs with constant stirring. The yellow coloured precipitate was generated by pouring the reaction mixture into ice cold water. The precipitate was filtered, washed thoroughly with distilled water and then recrystallized with ethanol. (Yield: 89%, M.P: 230 ^{o}C).

^{1}H–NMR ($CDCl_3$–d_1): δ ppm 10.30(s, –OH), 8.71(s, Ar–CH = N–), 7.99(d, Ar–CH), 7.86

(t, Ar–CH), 7.54(t, Ar–CH), 7.48(d, Ar–CH), 7.28(d, Ar–CH), 7.02(m, Ar–CH), 6.30

(t, Ar–CH). ^{13}C–NMR ($CDCl_3$–d_1): δ ppm 167.20(C8), 164.75(C7), 159.84(C1), 145.51(C9), 138.24(C3), 133.48(C5),131.95(C12), 131.61(C10), 130.23(C11), 129.30(C4), 126.44(C6), 117.08(C2). m/z (Found): 489.3784.

2.4. Synthesis of oligoesters

The monomer 2,2'–(((1,2–diphenylethane–1,2–diylidene)bis(hydrazine–2,1–diylidene))bis(methanylylidene))diphenolwas used to prepare oligoester by adopting procedure as follow [2]. The monomer (DBHMD: 1 g, 2.04 x 10^{-3} mole) was dissolved in chloroform and placed in ice bath. Into that, 0.52 ml (4.0 x 10^{-3} mole) of triethylamine was added dropwise followed by 0.79 ml (4.0 x 10^{-3} mole) phenylphosphonic dichloride and stirred for 1 hr at 0°C. The reaction mixture was warmed to room temperature and refluxed for 2 hrs. The reaction mixture was poured into the methanol and the precipitated oligoester was collected, washed with methanol and dried in a hot oven at 80°C for 24 hrs. The other oligoesters DMDOP and DMDAP were also synthesized by similar approach, using phenyl dichlorophosphate and adipoyl dichloride independently. The oligoesters are synthesized with satisfactory yields. (DMDMP: 83%, DMDOP: 87%, DMDAP: 81%).

DMDMP = (oligo(2,2'–(1,2–diphenylethane–1,2–diylidene)bis(hydrazine–2,1

–diylidene))bis (methaneylylidene))diphenol)phenyl phosphinate)

DMDOP = (oligo((2,2'–(1,2–diphenylethane–1,2–diylidene)bis(hydrazine–2,1

– diylidene))bis (methaneylylidene))diphenol))phenyl phosphonate)

DMDAP = (oligo((2,2'–(1,2–diphenylethane–1,2–diylidene)bis(hydrazine–2,1

– diylidene))bis (methaneylylidene))diphenol))adipate)

DMDMP: ^{1}H–NMR (DMSO–d_3): δ ppm 10.25 (s,–OH), 9.00(s,–CH = N), 7.99–6.86

(Ar–H). ^{13}CNMR (DMSO–d_3): δ ppm 163.14(C8), 159.16(C7), 146.05(C1), 144.57(C13), 138.90(C16), 135.15(C9), 133.70(C3), 131.97(C10), 130.98(C5), 129.85(C12), 127.84(C11), 126.72(C14) 124.88(C15), 123.83(C4), 120.57(C6), 111.24(C2). ^{31}P–NMR (DMSO–d_3):

δ ppm – 0.93, – 4.00, – 5.30–11.84, – 11.96, – 12.09, – 18.18.

DMDOP:^{1}H–NMR (DMSO–d_3): δ ppm 10.31 (s, –OH), 8.93(s,–CH = N), 7.98–6.76(Ar–H). ^{13}CNMR (DMSO–d_3): δ ppm 163.21(C8), 159.17(C7), 153.75(C1), 146.75(C13), 138.03(C9), 133.70(C5), 132.25(C3), 131.07(C15), 129.69(C12), 127.84C10), 126.66(C11), 125.23(C4), 123.55(C16), 120.54(C14), 118.74(C2), 109.82(C6). ^{31}P–NMR (DMSO–d_3): δ ppm 17.72.

DMDAP: ^{1}H–NMR ($CDCl_3$–d_1): δ ppm11.39 (s,–OH), 8.93 (s,–CH = N), 8.72–6.77

(Ar–H), 2.37(d, Ha), 1.69(t, Hb). ^{13}C–NMR ($CDCl_3$–d_1): δ ppm197.47(C13), 167.62(C8), 160.53(C7), 151.18(C1), 142.15(C5), 135.70(C9), 133.88(C12), 132.80(C10), 131.68(C11), 129.03(C3), 128.32(C2), 114.83(C4), 110.84(C6), 55.87(C14), 33.53(C15).

2.5. Results and discussion

2.51. Solubility

The solubility of synthesized compounds was tested with different solvents such as methanol, DMF, n–hexane, ethyl acetic acid, DMSO, ethanol, THF, CH_2Cl_2, acetonitrile, acetone and $CHCl_3$ in room temperature. For this study, 0.1g of substance was used to test the solubility in 1 ml of above-mentioned solvents. The synthesized compounds are fully soluble in DMSO, DMF and THF, but only slightly soluble in $CHCl_3$, ethyl acetate and CH_2Cl_2. The compounds are insoluble in non–polar solvents. In oligoesteric reaction, most of the phenolic –OH groups are involved and therefore oligoesters have less solubility than the monomer DBHMD. The solubility of oligoesters in highly polar DMSO may be due to the terminal polar –OH group [29].

2.52. Molecular weight (Gel permeation chromatography)

The gel penetration chromatography was used to determine the molecular weight of the oligoesters and the chromatogram of oligoestersare given in SF. 1. The polystyrene standard calibration curve was used to calculate the number average molecular weight (Mn), weight average molecular weight (Mw) and polydispersity index (PDI) of DMDMP, DMDOP and DMDAP oligoesters.

Mn, Mw and PDI are 2415, 2178 g mol^{-1} and 1.10 for DMDMP, 2134, 1895 g mol^{-1} and 1.12 for DMDOP and 2015, 1976 g mol^{-1} and 1.01 for DMDOP respectively. The low PDI value of the oligoesters indicate the presence of less number of branches and structural homogeneity in the chain [4].

2.53. Spectral Characterizations

SF. 2 depicts the FT–IR spectra of monomer and oligoesters, and their spectral data are listed in Table 2. In the FT–IR spectra, the bands appeared at 1483–1456 cm^{-1} and 1690–1598$cm^{-1}$are indicating the presence of > C = C < and > C = N < stretching vibration of monomer and oligoesters. The monomer's phenolic –OH stretching vibration and the end –OH group stretching of oligoesters are found at about 3520 and 3553–3420cm^{-1} respectively. The C–H stretching vibration appears at 3172 and 2985–2977 cm^{-1} for monomer and oligoesters respectively.

Table 1
Solubility of monomer and oligoesters

Compound	DMSO	DMF	THF	$CHCl_3$	CH_2Cl_2	CH_2CN	MeOH	EtOH	n–hexane	Acetone
DBHMD	+	+	+	+	+	+	±	±	–	–
DMDMP	+	+	+	±	±	–	–	–	–	–
DMDOP	+	+	+	±	±	–	–	–	–	–
DMDAP	+	+	+	±	±	–	–	–	–	–
Soluble: +, Partially soluble: ±, **Insoluble: –**										

Table 2
FT–IR spectral data of monomer and oligoesters

Compounds	Wavenumber(cm^{-1})							
	–OH	–C = N–	–C = C–	Ar–H	P–O–C	P = O	O = P–OH	–C = O
DBHMD	3520	1690	1465	3172	–	–	–	–
DMDMP	3537	1645	1456	2979	1155	1279	2688	–
DMDOP	3553	1598	1474	2977	1198	1266	2692	–
DMDAP	3420	1609	1483	2985	–	–	–	1726

The bands that occurred at 2692–2688, 1198–1155 and 1279–1266 cm^{-1} for O = P–OH, P–O–C and –P = O confirm the presence of phosphorous in DMDMP and DMDOP oligoesters structure. Similarly, the band appeared at 1726 $cm^{-1,}$ indicating the > C = O stretching vibration and providing evidence for ester linkage in DMDAP oligoester structure [5].

^{1}H and ^{13}C–NMR spectra of the monomer are shown in SF. 3. In the ^{1}H–NMR spectrum, the azomethane, hydroxy proton and aromatic proton chemical shift appear at 8.71, 10.30 and 7.99–6.95 ppm respectively. The aromatic proton shifts in DBHMD are comparatively higher than the 2BH hydrazone. The disappearance of $-NH_2$ chemical shift around 6.00 ppm in the DBHMD spectrum is strongly indicating the formation of the expected structure. The chemical shift of carbon atoms in various chemical environments of DBHMD are displayed in ^{13}C–NMR spectrum. DBHMD exhibits an additional azomethane chemical shift at around 165.42 ppm compared to hydrazone is indicating the formation of the expected azine structure. Furthermore, the DBHMD high resolution mass spectrum (SF. 4) shows m/z value at 489.3784, confirming the monomer structure.

SF. 5 show the ^{1}H and ^{13}C–NMR spectra of oligoesters. The chemical shift of azomethine proton in the oligoesters appear in the range 8.94–8.51 ppm. The azomethane proton shift appear at slightly downfield than the monomer due to the deshielding effect of additional phenyl rings [30].

The chemical shift occurred at 11.39–10.31 ppm, indicating the presence of terminal

–OH group in the oligoesters. The presence of more chemical shift values than the monomer in the aromatic region implies the incorporation of phenyl groups in DMDMP and DMDOP oligoesters' backbone. Similarly, DMDAP oligoester exhibits additional proton chemical shift in the aliphatic region at 2.37–1.57 ppm and the terminal –OH group in the higher chemical shift value(11.39 ppm) confirm the structure of DMDAP oligoester[7].

In the ^{13}C–NMR spectra, due to the incorporation of phenyl groups into the backbone of oligoesters results in more chemical shift than the monomer. The appearance of additional chemical shift at 197.47 ppm corresponding to ester carbon and 42.12–11.89 ppm for the aliphatic carbon supports the DMDAP oligoester structure.

The ^{31}P–NMR spectra of oligoesters are shown in SF. 6. The spectra show significant chemical shifts at − 0.93 to − 18.18 ppm and17.72 ppm respectively. The negative and positive chemical shift values respectively indicates the presence of phosphorous in the main and end group of the oligoesters chain[31], which confirms the phosphorous incorporation in the oligoester chain's backbone [32].

2.5.4. Thermogravimetric analysis

The thermogravimetric analysis was performed in nitrogen atmosphere at a heating rate of 10°C/min and the thermogram is shown in SF. 7. The oligoesters DMDMP, DMDOP and DMDAP are stable up to 126, 131 and 123°C respectively. Table 3 shows the 10% and 50% weight loss and their char residue at 600°C.The initial weight loss of the oligoesters' occurred around 100^{o}C are due to the exclusion of accumulated water molecules.The second stage degradation of DMDMP, DMDOP and DMDAP in the range 182–200^{o}C may be due to degradation of the ester group from the structure. The final degradation that occurred at

Table 3
TGA data of oligoesters

Compounds	10% weight loss	50% weight loss	% of Residual at 600(ºC)	LOI
DMDMP	154	361	40	33.5
DMDOP	155	291	43	34.7
DMDAP	162	282	34	31.1

300–427C may be due to the breaking of main chain of oligoesters [].

The char yield is an essential factor in determining the polymer's limiting oxygen index (LOI). The LOI of oligoesters were calculated using Van Krevelen and Hoftyzer equation [34]LOI = 17.5 + 0.4CR (Char yield).The LOI values of oligoesters are less than 45. DMDOP has greater LOI value among the oligoesters, resulting in decreased flammability and higher

self–extinguishing property[35].

2.5.5 Contact angle measurement of monomer

The contact angle(θ) water equilibrium of DBHMD has been investigated and is shown in SF. 8. The water contact angle on the DBHMD surface is 87 ± 1^{o}. The result demonstrates the hydrophilic nature of monomer[12, 13].

2.5.6. Optical properties

The UV–Vis and fluorescence spectra of monomer and oligoesters in DMF solution are shown in SF. 9. The Tauc diagram was used to calculate the band gap value of monomer and oligoesters. In the absorption spectra, the bands appear at 251–255 and 304–312 nm representing the π–π* and n–π* transition respectively. The absorbance band appeared at

359–377 nm is due to the ground state electron transfer between phenolic –OH and azine nitrogen in ground state(–C = N–)[38].

The absorbance band of the oligoesters appeared at lower wavelength than that of the monomer. This hypsochromic shift from their monomer absorption wavelength is due to the changes in the planarity of oligoesters in the backbone. The absorbance wavelength of DMDAP appeared at higher wavelength than DMDMP and DMDOP is due to the presence of high π—π stacking interaction between the repeating units [39]. The band gap value of monomer and oligoesters calculated using Tauc method are 2.96, 3.21, 3.16 and 3.03 eV for DMDMP, DMDOP and DMDAP respectively. The formationof ester linkage causes the lack of conjugation in the repeating unit of oligoester, resulting in lower absorption wavelength and higher band gap value than the monomer [40].

In the fluorescence investigation, the excitation wavelength of monomer and oligoesters were fixed at their respective absorption wavelength. The emission bands appeared at 387, 456 nm for DBHMD 391,461 nm for DMDMP, 385, 459 nm for DMDOP and

394, 466 nmfor DMDAPrespectively. The dual emission appeared in excited state is due to the formation of keto enol tautomer through the ESIPT process. The Stoke's shift ($\Delta\lambda_{ST}$) value occurred due to the relaxation of excited electrons or structure relaxation of the compound.

The Stoke's shift value is 79 for DBHMD and 102, 94, and 95 for DMDMP, DMDOP and DMDAP respectively. The elongation of the double bond in the oligoester chain causes larger Stoke shift value than monomer [41]. The absorption, emission and Stoke's shift value of monomer and oligoesters are listed in Table 4. The high Stoke's shift value reduces the overlapping of the excitation–emission spectra and reduces the background signal. So, the molecule with high Stoke's shift value can be an excellent fluorescence sensor [42].

Table 4
Fluorescence spectral data of monomer and oligoesters

Compound	Absorption		Emission	
	$\lambda_{max(nm)}$[a]	$Eg_{(eV)}$[b]	$\lambda_{max(nm)}$[c]	$\Delta\lambda_{ST}$[d]
DBHMD	251,309,377	2.96	387,456	79
DMDMP	253,307,359	3.21	391,461	102
DMDOP	255,312,362	3.16	385,459	97
DMDAP	252,304,371	3.03	394,466	95
[a]Absorption maximum, [b]Band gap, [c]Emission maximum,				
[e]Stoke's shift				

The intramolecular proton transfer from phenolic –OH to azine (= N–N=) in the excited state causes dual emission in the fluorescence spectra of monomer and oligoesters.

The DBHMD was taken to explain the ESIPT process, which contains azine nitrogen ortho to phenolic group. The reduced density gradient (RDG) was used to find out the weak and strong hydrogen bonding interactions in the molecule, which are plotted against sign(λ_2)ρ) are shown in Fig. 1. According to Johnson et al. approach, the positive sign(λ_2)ρ denotes steric effects, the negative sign(λ_2)ρ signifies hydrogen bonding interactions and van der Waals effects of the molecules and are assigned values near zero[43]in the RDG image. The spikes that appeared from − 0.05 to − 0.04 in the RDG image of the monomer indicate a strong intramolecular hydrogen bonding contact in the ground state (S_0) between the phenolic O–H and azine (= N–N=) nitrogen. The schematic representation of fluorescence emission ESIPT keto–enol tautomerism of DBHMD is depicted in SF. 10.

According to Kasha's rule, only the lowest initial excited state following electronic depletion and vibrational relaxation can cause to perform photochemical reactions or fluorescence emission. The lowest unoccupied molecular orbital (LUMO) and highest occupied molecular orbital (HOMO) are highly related to proton transfer (LUMO)[44].

The O–H charge density decreases when the charge is transported from the HOMO to LUMO in the excited state, causing increase in the charge density of the azine nitrogen

(–N=). In the excited state, the hydroxy protons are highly attracted by the high charged density azine nitrogens, leading to keto–enol tautomerism [45]. The theoretical FT–IR spectrum of DBHMD was performed and is shown in SF.11. In this spectrum, the O–H stretching vibration appears at 3752.45 and 3179.96 cm^{-1}. The appearance of band at longer wavenumber is confirming the –OH stretching vibration. The strong interaction between hydroxy O–H and azine nitrogen weakens the stretching vibration of O––H ((O–––H–––N)) and shows the band at lower wavenumber confirming the intramolecular proton interaction.

2.5. Chemosensor studies

2.5.1. Evaluation of selectivity

The selectivity of fluorophores (DBHMD, DMDMP, DMDOP and DMDAP), was investigated with the different metal ions in DMF/H_2O solution (1:1, pH: 7.4, fluorophore: 5μM). The fluorescence of free fluorophores and fluorophores added with different metal ions such as nitrate salts of Ag^{+}, Pb^{2+}, Ba^{2+}, Ca^{2+}, Al^{3+}, Bi^{3+}, Mg^{2+}, Na^{+}, Cr^{3+}, Ni^{2+}, Ce^{3+}, Zr^{2+}, Zn^{2+}, Mn^{2+}, Cd^{2+}, Li^{+}, Co^{2+}, Hg^{2+} and chlorides salts of La^{3+}, Fe^{3+}, Cu^{2+}, Fe^{2+}, K^{+} were studied. In this study, the fluorescence intensity of fluorophore was efficiently quenched by Cu^{2+} ion and shows good ‘on off’ response than the other metal ions as shown in Fig. 2. The quenching occurred due to the paramagnetic behaviour and d–π interaction between the fluorophore and Cu^{2+} ion [46]. All fluorophores exhibit good quenching response with Cu^{2+} ion. Oligoesters show higher fluorescence intensity quenching than the monomer due to its strong binding and more binding sites for Cu^{2+} ions.

2.5.2. Competitive analysis with other metals

The effective chemosensors should sense the particular metal ion without interfering with other metal ions. Therefore, in the competitive study, the fluorophores were individually studied with Cu^{2+} ion over the presence of other metal ions in 100 equivalents. The results illustrate that the fluorophores have no significant change in their fluorescence intensity over the presence of other metal ions. The results show the selective response of fluorophores towards Cu^{2+} ion. Further the fluorophores are able to detect Cu^{2+} independent ofthe presence of other competing metal ions (Chloride of Ag^{+}, K^{+}, La^{3+}, Fe^{2+}, Fe^{3+} and nitrate of Ba^{2+}, Al^{3+}, Bi^{2+} Pb^{2+}, Cd^{2+}, Hg^{2+}, Cr^{3+}, Ce^{3+}, Li^{+}, Zn^{2+}, Zr^{2+}, Mn^{2+}, Mg^{2+}, Co^{2+}, Ni^{2+}, Ca^{2+}, Na^{+}).

Figure 3 illustrates the fluorescence response of the fluorophores with Cu^{2+}in the presence of other metal ions.

2.5.3. Quenching response towardsCu^{2+}ion concentration

The fluorophores were investigated with various concentrations of Cu^{2+} ion separately in DMF/H_2O solution. Their fluorescence intensity gradually decreases with increase in concentrations of Cu^{2+} ion. Upon the addition of Cu^{2+} ion into the fluorophore solution quenched the fluorescence intensity due to the interaction between Cu^{2+} ion and fluorophore by energy or electron transfer process [47].

The quenching responses of fluorophores are shown in Fig. 4. The ground state interaction between Cu^{2+} ion and fluorophore is revealed by comparing the fluorophore–Cu^{2+} and fluorophores’ absorption spectrum and is shown in SF. 12. The bathochromic shift observed from their actual absorption band isindicating the ground state interactions between the fluorophores and Cu^{2+} ion. The interaction of Cu^{2+} ion with the electron withdrawing acceptors group causes the red shift in the absorption spectrum[48].

Stern–Volmer plot and limit of detection

The obtained quenching data of fluorophores with Cu^{2+} ion was used to calculate the limit of detection (LOD) and binding stoichiometry. The binding stoichiometry of fluorophores with Cu^{2+} ion was calculated using the Stern–Volmer equation (I_0/ I = 1 + Ksv [Q]).

Here, I and I_0 are the fluorescence intensities of fluorophore in the presence and absence of quencher. The Stern–Volmer constant is Ksv and [Q] is the concentration of the quencher[49]. A graph is plotted with relative fluorescence intensity (I_0/ I) against the concentration of $Cu^{2+}$and is shown in Fig. 5. The dynamic and dominant diffusion process is taken place in the fluorophores solution upon the addition of Cu^{2+} ion [50]. From the Stern–Volmer plot, the correlation coefficient (R^2) values calculated are 0.99769, 0.99711, 0.99396 and 0.99510 for DBHMD, DMDMP, DMDOP and DMDAP respectively.The results illustrated the fluorophores' capability to determine Cu^{2+} ion quantitatively in the solution. The fluorophores LOD value towards Cu^{2+} ion was calculated using the formula LOD = 3.3σ/k. Where k is the slope of the calibration graph and σ is the y–intercept of the regression line [51]. The detection limit was calculated and is 1.62 x 10^{-8}, 3.89 x 10^{-8}, 1.90 x 10^{-8} and 5.86 x 10^{-8} M for DBHMD, DMDMP, DMDOP and DMDAP respectively.

Benesi–Hildebrand plot

The binding constant (Ka) of the fluorophore with Cu^{2+} ion was calculated from the linear fitting curve of Benesi–Hildebrand plot and is shown in Fig. 6. The Binding constant values calculated are 1.0012, 1.0018, 1.0015 and 1.0014 M^{-1} for DBHMD, DMDMP, DMDOP and DMDAP respectively. The results indicates the high binding capability of fluorophores toward Cu^{2+} ion in the chemosensor study.

2.5.4. Time effect

The spot response is an essential property of fluorophores to detect the respective metal ion at a particular time. So, the fluorophores were examined with Cu^{2+} ion in DMF/H_2O solution(1:1, fluorophore = 5μM, pH = 7.4) at different periods. The addition of Cu^{2+} ion into the fluorophore solution causes fluorescence quenching and increasing with increase in the contact time and attaining maximum quenching around 5 minutes. The effect of time on the fluorescence quenching is depicted in Fig. 7.The quick response of decrease in fluorescence intensity of fluorophores with the addition of Cu^{2+} ion indicates the capability of fluorophores to detect the Cu^{2+} ions in real time[52].

2.5.5. Sensor efficiency versus pH

The fluorescence response and sensing capability of fluorophores with and without metal ions were investigated in DMF/H_2O solution (1:1, fluorophore = 5M) at different pH from 1 to 13. The pH of the solution was adjusted with 0.1 M HCl and 0.1 M NaOH solution. The electron transition from azine to a phenyl ring and vice versa is maximum at high and low pH levels due to formation ionic structure in the fluorophores [53].

At higher pH level, the equilibrium between phenolic and phenoxide is shifting the equilibrium towards the phenoxide formation. This formation of phenoxide increases the conjugation in the fluorophore system and reduces the HOMO–LUMO band gap value. So less energy is required to transfer an electron from lower to higher energy and increase the fluorescence intensity [54]. The effect of different pH on fluorophores' detection efficiency with Cu^{2+} ion is illustrated in SF. 13.

2.5.6. Reversible capability of chemosensor

The fluorophores' reversibility is an essential property of chemosensors to detect the metal ion in many cycles. The study was carried out by adding ethylenediaminetetraacetic acid (EDTA) in to fluorophore–Cu^{2+}solution (1:1, fluorophore = 5M, pH = 7.4). The fluorescence intensity of fluorophore–Cu^{2+} gradually increases with the addition of EDTA into the fluorophore solution. The fluorophores' quenching intensity is completely nullified with 100 equivalents of EDTA. The outcome demonstrates an excellent reversibility of fluorophores with EDTA and show that the fluorophores can be used multiple times to detect the Cu^{2+} ion. The results are shown in Fig. 8.

2.6. Computational method

The structural parameters of fluorophore and quencher were determined using density functional theory (DFT). The dimer of fluorophores and quencher structure were optimized in the B3LYP/6–311 + + G(d,p) and LANL2DZ basis set the results are shown in SF. 14.

2.6.1. Frontier molecular orbital analysis

The bandgap value ofmonomer and dimer of oligoesters were calculated using frontier molecular orbital analysis. The energy value of HOMO and LUMO are used to measure the optical polarizability, chemical hardness–softness and chemical reactivity of the

molecules[55]. Generally, the small band gap molecules are stable with low excitationenergy and chemical hardness. The band gap value of DBHMD, DMDMP, DMDOP and DMDAP are 3.3478, 3.4011, 3.4128 and 3.3244eV respectively.

The molecules' polarizability highly depends on the softness and hardness of the molecules, which is calculated by the formula [56] is, = 1/2(A–I). Here, the I and A are

E_{HOMO} and E_{LUMO} energy of molecules. The η value of DBHMD is found to be 1.6739 eV and for the dimer of DMDMP, DMDOP and DMDAP oligoesters are 1.7005, 1.7064 and 1.6622 eV respectively. The band gap value of the quencher is found to be 2.9132eV.

The Frontier molecular orbital images of oligoesters dimer and quencher are shown in

SF. 15 and 16 respectively and their values are listed in Table 5.

Table 5
HOMO LUMO and band gap value of ligand and metal

Compound	E_{HOMO}	E_{LUMO}	Band Gap(eV)	MO. Number
DBHMD	−6.0483	−2.7004	3.3478	117(O), 118(U)
DMDMP	−5.9996	−2.5984	3.4011	265(O), 266(U
DMDOP	−6.0382	−2.6253	3.4128	269(O), 270(U
DMDAP	−6.0888	−2.7644	3.3244	263(O), 264(U
$Cu(OH)_2$	−7.6500	−4.7368	2.9132	18(O), 19(U
O, U = Occupied and Unoccupied orbital				

At higher pH Cu^{2+} is hydrated and forming $Cu(OH)_2$.Thestructure of $Cu(OH)_2$ was optimised and the band gapvalue isfound to be 2.9132eV from its HOMO–LUMO energy values. The chemical hardness value of the quencher calculated is1.4566 eV. The low chemical hardness generally indicates less resistance to the charge transfer process [57].

The energy difference between LUMO and electrophilicity index of fluorophore and quencher indicates the possibility of making a bond through the electron or charge transfer process.

2.6.2. Molecular electrostatic potential (MEP) and contour map

Different colours represent the negative and positive sites of the fluorophores on the MEP surface. The blue and red colours indicate the positive (electrophilic reactivity) and negative (electrophilic reactivity) sites, other colours on the map represent the neutral sites of the fluorophore molecule. The MEP and contour map are indicating the more susceptible sites in the molecule to nucleophilic and electrophilic attack. The MEP and contour map are shown in SF. 17 and 18 respectively.

The image exhibits that oxygen and nitrogen have higher electronegativity than the other atoms in the molecule. The contour map shows the maximum electron flow in the molecule, which is higher around nitrogen and oxygen than on other atoms in the molecule. Further, the local and global descriptors were studied to confirm the feasible binding sites in the molecule for the electrophilic and nucleophilic attacks with metal ion in the chemosensor study.

2.6.3. Global descriptors

In Koopmans' theorem, the energy values of HOMO and LUMO were used to determine global descriptors such as the global hardness (η), electrophilic index (ω), chemical potential (μ), electronegativity (χ) and global softness (S) of the molecule [58]. The E_{HOMO} and E_{LUMO} energy values are indicated as A and I.Table 6. shows the global descriptors of the molecule derived using the above equation.

Table 6
Global descriptors values of fluorophores and quencher

Compound	I $=E_{HOMO}$	A $= E_{LUMO}$	X $=(I+A)/2$	$= 1/2(A-I)$	$=-\chi$	$= 1/2\eta$	$=\mu^2/2\eta$	ΔN_{max} $=-\mu/\eta$
DBHMD	−6.0483	−2.7004	4.3744	1.6739	−4.3744	0.8369	5.7157	2.6132
DMDMP	−5.9996	−2.5984	4.2990	1.7005	−4.2990	0.8502	5.4338	2.5279
DMDOP	−6.0382	−2.6253	4.3318	1.7064	−4.3318	0.8532	5.4981	2.5385
DMDAP	−6.0888	−2.7644	4.4266	1.6622	−4.4266	0.8311	5.8942	2.6630
$Cu(OH)_2$	−7.6500	−4.7367	6.1933	1.4566	−6.1933	0.7283	13.1670	4.2519

$\chi = -(I + A)/2$

$= 1/2(A-I)$

$S = 1/2$

$\mu = -\chi = (I + A)/2$

$= \mu^2/2$

ΔN max $= -\mu/$

The stabilization energy of the system while adding or removing electrons from the environment was determined by measuring the electrophilic index ( ) value [59]. The low chemical potential value and high electrophilicity index value indicate the electrophilic behaviour of the system [60]. Comparatively, the quencher has higher electrophilicity index value and the energy difference between the chemical potential and electrophilicity index is higher, indicating its strong electrophilic behaviour. Moreover, fluorophoresare having higher LUMO value than quencher. Therefore, fluorophores can easily transfer the electrons to the lower LUMO of quencher. Further confirming the electron or charge transfer process following descriptors were studied.

Electrophilicity based charge transfer descriptors (ECT)

The charge transfer in the molecules was calculated using the charge difference between quencher(M^+) and fluorophores(F). The charge transfer descriptor(ΔN_{max}) was calculated using the formula [61],

$ECT = (\Delta N_{max})F - (\Delta N_{max})M^+$

When, F and M^+ approach the charge flow from M^+ to F, if ECT > 0, the charge flows from F to M^+ if ECT < 0. ECT values of the DBHMD, DMDMP, DMDOP and DMDAP are

−1.63 − 1.72, − 1.71 and − 1.58 respectively. The ECT values of fluorophores indicate that the charge flows from F to M^+. The DMDMPfluorophore has lower electronegativity (χ) and ECT values than the other fluorophores indicating the ability to interact with metal ions through the LMCT process in the chemosensor study.

2.6.4. Local descriptors

The local descriptors are mostly used to determine the molecule's exact binding sites or reactive sites. Here, the local descriptors for fluorophores were studied to determine the exact binding sites with the metal ion in the chemosensor study. The Yang and Mortier [62] method was used to calculate the Fukui functions (f_{k+}, f_{k-}, f_{k0}) with the following equations,

$f_k^0 = 1/2[q(N+1) - q(N-1)]$ – For radical attack

$f_k^+ = [q(N+1) - q(N)]$ – For nucleophilic attack

$f_k^- = [q(N) - q(N-1)]$ – For electrophilic attack

The molecules' neutral, anionic, and cationic states are represented as N, N−1, and N + 1.

Local softness

The exact reactivity site of the fluorophore molecules was described using local electrophilic index (ω_k^+, ω_k^- and ω_k^0) and local softness (S_k^+, S_k^- and S_k^0) of the fluorophore molecules. The results are listed in Table 7. Here, +, 0 and − indicate nucleophilic, radical and electrophilic attacking sites of the fluorophores system. The atoms highlighted in the Table withhigher electrophilicity index than the other atoms indicate feasible and more prone site to electrophilic attack [38, 24] in the chemosensor study. The possible binding site of the fluorophore with Cu^{2+} ion is shown in Fig. 9.

Table 7
Local descriptors values of fluorophores

Compound	Atoms	Natural atomic charges (eV)			Fukui functions(eV)			Local softness(eV)			Local electrophilicity index(eV)		
		qN + 1	qN0	qN−1	f_k^+	f_k^0	f_k^-	S_k^+	S_k^0	S_k^-	$_k^+$	$_k^0$	$_k^-$
DBHMD	8 N	0.320	0.480	−0.195	−0.161	0.257	0.675	−0.134	0.215	0.565	−0.91	1.470	**3.858**
	9 N	0.138	−0.042	−0.270	0.180	0.204	0.228	0.151	0.171	0.191	1.028	1.166	1.304
	12 N	0.245	0.160	−0.242	0.085	0.244	0.403	0.071	0.204	0.337	0.486	1.394	2.302
	13 N	0.122	0.141	−0.385	−0.019	0.253	0.526	−0.016	0.212	0.440	−0.10	1.448	3.006
	21 O	0.311	0.226	−0.219	0.085	0.265	0.445	0.071	0.222	0.372	0.486	1.514	2.543
	22 O	0.182	0.148	−0.217	0.034	0.200	0.365	0.028	0.167	0.306	0.194	1.141	2.088
DMDMP	8 N	−0.165	0.593	0.457	−0.758	−0.31	0.136	−0.644	−0.264	0.115	−4.117	−1.690	0.737
	9 N	−0.212	−0.127	−0.039	−0.085	−0.08	−0.08	−0.073	−0.074	−0.07	−0.464	−0.472	−0.480
	12 N	−0.180	−0.157	0.168	−0.023	−0.17	−0.32	−0.020	−0.148	−0.27	−0.125	−0.947	−1.769
	13 N	−0.191	0.838	0.190	−1.028	−0.19	0.648	−0.874	−0.162	0.551	−5.588	−1.034	**3.520**
	63 N	−0.183	0.635	0.551	−0.818	−0.36	0.084	−0.695	−0.312	0.071	−4.444	−1.994	0.455
	64 N	−0.187	−0.015	−0.038	−0.172	−0.07	0.022	−0.146	−0.064	0.019	−0.935	−0.407	0.122
	67 N	−0.199	0.272	0.158	−0.471	−0.17	0.113	−0.400	−0.152	0.096	−2.559	−0.971	0.617
	68 N	−0.368	0.101	0.130	−0.469	−0.24	−0.02	−0.399	−0.212	−0.02	−2.550	−1.354	−0.159
	76 O	−0.159	0.219	0.223	−0.378	−0.19	−0.04	−0.322	−0.162	−0.03	−2.056	−1.038	−0.019
	77 O	−0.740	0.237	0.247	−0.977	−0.49	−0.01	−0.831	−0.419	−0.08	−5.307	−2.680	−0.052
	122 P	1.523	−1.331	−1.462	2.854	1.492	0.131	2.427	1.269	0.111	15.507	8.110	0.712
	123 O	−0.656	0.034	0.109	−0.689	−0.38	−0.07	−0.586	−0.325	−0.06	−3.746	−2.077	−0.408
DMDOP	8 N	−0.167	0.510	0.340	−0.677	−0.25	0.170	−0.577	−0.216	0.145	−3.720	−1.393	**0.934**
	9 N	−0.213	−0.101	0.019	−0.115	−0.11	−0.11	−0.098	−0.099	−0.10	−0.632	−0.638	−0.645
	12 N	−0.173	−0.041	−0.132	−0.132	−0.02	0.091	−0.112	−0.017	0.078	−0.724	−0.112	0.500
	13 N	−0.173	0.767	0.826	−0.940	−0.49	−0.05	−0.802	−0.426	−0.05	−5.168	−2.745	−0.323

	21 O	– 0.771	0.246	0.263	– 1.017	– 0.51	– 0.01	– 0.868	– 0.441	– 0.01	– 5.592	– 2.843	– 0.094
	22 O	– 0.181	0.153	0.138	– 0.334	– 0.15	0.015	– 0.285	– 0.136	0.013	– 1.835	– 0.876	0.082
	63 N	– 0.187	0.547	0.414	– 0.734	– 0.30	0.133	– 0.627	– 0.256	0.114	– 4.038	– 1.652	0.733
	64 N	– 0.188	0.048	0.108	– 0.236	– 0.14	– 0.06	– 0.201	– 0.126	– 0.05	– 1.298	– 0.815	– 0.331
	67 N	– 0.199	0.253	0.324	– 0.452	– 0.26	– 0.07	– 0.386	– 0.223	– 0.06	– 2.485	– 1.439	– 0.393
	68 N	– 0.368	0.139	– 0.022	– 0.506	– 0.17	0.160	– 0.432	– 0.148	0.137	– 2.784	– 0.951	0.882
	76 O	– 0.157	0.235	0.207	– 0.392	– 0.18	0.028	– 0.335	– 0.155	0.024	– 2.157	– 1.001	0.154
	77 O	– 0.722	0.432	0.407	– 1.154	– 0.56	0.024	– 0.984	– 0.482	0.021	– 6.343	– 3.105	0.133
	122 P	0.144	0.037	0.268	4.395	2.261	0.128	3.749	1.930	0.110	24.162	12.434	0.706
	123 O	1.693	– 2.701	– 2.830	– 0.869	– 0.42	0.027	– 0.741	– 0.359	0.023	– 4.777	– 2.313	0.151
	124 O	– 0.662	0.207	0.179	– 1.028	– 0.51	– 0.04	– 0.877	– 0.441	– 0.04	– 5.654	– 2.839	– 0.024
DMDAP	8 N	0.505	0.805	0.860	– 0.301	– 0.17	– 0.05	– 0.250	– 0.148	– 0.04	– 1.773	– 1.050	– 0.327
	9 N	0.102	– 0.261	– 0.165	0.363	0.134	– 0.09	0.302	0.111	– 0.08	– 2.141	0.787	– 0.566
	12 N	0.208	– 0.123	0.146	0.331	0.031	– 0.26	0.275	0.026	– 0.22	1.951	0.182	– 1.586
	13 N	0.178	0.527	0.175	– 0.350	0.001	0.353	– 0.291	0.001	0.293	– 2.062	0.008	**2.078**
	21 O	0.029	0.029	0.001	– 0.004	0.014	0.028	0.000	0.011	0.023	– 0.002	0.080	0.163
	22 O	0.189	0.122	0.091	0.067	0.049	0.031	0.056	0.041	0.026	0.397	0.290	0.184
	63 N	0.357	0.364	0.314	– 0.008	0.021	0.050	– 0.006	0.018	0.042	– 0.046	0.126	0.297
	64 N	0.159	0.155	0.142	0.004	0.008	0.013	0.003	0.007	0.010	0.025	0.049	0.074
	67 N	0.288	0.270	0.246	0.017	0.021	0.024	0.014	0.017	0.020	0.102	0.122	0.142
	68 N	0.103	0.075	0.027	0.028	0.038	0.048	0.023	0.032	0.040	0.166	0.224	0.283
	76 O	0.257	0.219	0.201	0.038	0.028	0.018	0.032	0.023	0.015	0.225	0.165	0.105
	77 O	0.234	0.249	0.211	– 0.016	0.011	0.039	– 0.013	0.010	0.032	– 0.094	0.067	0.229
	117 O	– 0.112	– 0.150	– 0.144	0.038	0.016	– 0.05	0.032	0.014	– 0.04	0.223	0.096	– 0.031
	118 O	0.010	0.010	– 0.020	3E0– 5	0.015	0.030	2E0– 5	0.012	0.025	0.001	0.087	0.175

2.7. Mechanism of sensing

The ground state interaction between fluorophore and quencher is explained with results of UV–Vis spectroscopy. Fluorescence ‘turnoff’ mechanism is explained using fluorescence spectrum of fluorophores with 100 equivalents of Cu^{2+} ion and DFT results of the

fluorophores and quencher. In the excited state, the hydroxyl protons are attracted by high electron density azine nitrogen,inducing ESIPT process and transfer proton from hydroxyl to azine nitrogen giving dual emission in the fluorescence spectrum. The fluorophore with Cu^{2+}ion causes interaction in the ground state, which is confirmed by the bathochromic shift of fluorophore from its actual absorption band. The absorption band shifts and ECT results demonstrate the ground state interaction that occurred via the ligand to metal charge transfer (LMCT) process [64].

The higher LUMO value of fluorophores has greater possibility of transferring an electron to the lower LUMO of the quencher. Moreover, the obtained negative values in the ECT give evidence to the LMCT process. The LMCT process leads to bathochromic shift in the ground state due to the attraction of electron withdrawing group of fluorophore and paramagnetic effect of quencher, stalling the PET and induced reverse PET process causing fluorescence quenching in the chemosensor study. The 'turn off' mechanism of fluorophores with Cu^{2+} ions is shown in Fig. 10.

2.8. Water sample analysis

The practical applicability of fluorophores was examined for the real models using two lake water samples collected from Kurichikulam (KW) and Periyakulam (PW) in Ukkadam, Coimbatore, Tamil Nadu, India. The detection of Cu^{2+} ion in these samples was evaluated by spiking a known concentration of Cu^{2+} ion and estimating the recovery.Table 8 shows the significant recovery from the three repeated measurements in spiked water samples. The results show that fluorophores can detect Cu^{2+} ions in natural water samples.

Table 8
Detection of Cu^{2+} in spiked water samples using fluorophores

Compound	Sample	Cu^{2+} spiked (μM)	Cu^{2+}found (μM) mean[a] ± SD[b]	Recovery (%)	Relative error (%)
DBHMD	LW 1	5	5.08 ± 0.08	101.3	1.3
		10	9.89 ± 0.11	98.3	−1.7
	LW 2	5	4.96 ± 0.04	99.2	−0.8
		10	9.95 ± 0.05	99.5	−0.5
DMDMP	LW 1	5	5.05 ± 0.05	100.5	0.5
		10	9.93 ± 0.07	99.2	−0.8
	LW 2	5	4.95 ± 0.05	98.7	−1.3
		10	9.90 ± 0.10	99.0	−0.1
DMDOP	LW 1	5	5.10 ± 0.10	101.8	1.8
		10	9.92 ± 0.08	99.1	−0.9
	LW 2	5	4.98 ± 0.02	99.7	−0.3
		10	9.99 ± 0.01	99.5	−0.5
DMDAP	LW 1	5	5.04 ± 0.03	100.4	0.4
		10	9.92 ± 0.08	99.1	−0.9
	LW 2	5	4.96 ± 0.04	99.5	−0.5
		10	9.98 ± 0.02	99.8	−0.2

[a] mean of three measurements, [b] standard deviation

2.9. Cell imaging analysis

Before the cell imaging experiments, the highly responsive fluorophore DMDMP with and without Cu^{2+} ion was tested for cytotoxicity against the blood cancer Human monocytic leukemia cells (THP–1).The cells were incubated for 24 hrs at 37°C with different concentrations (0, 0.5, 1, 2, 3, 4 and 5 mg/ml) of DMDMP and DMDMP –Cu^{2+},then MTT (5mg/ml) was added to the treated cells and incubation continued for further 4 hrs.

The fluorophore DMDMP and DMDMP–Cu^{2+}show 91.06 and 93.86% survival rate of cancer cells at 5mg/ml. For the excitation 408, 488, 520 and 630 nm Laser were used. The result shows that the cells stained with the compounds does not show any fluorescence or adverse change in morphologyresulting in the absence of the expected fluorescent images. The cell imaging investigation is illustrated in SF. 19. The fluorophore are not toxic to the cells, has low ability to penetrate the cell and suitable mode of delivery the molecules can enter the cell and stain them, preferably without toxic side effect.

2.10. DC electrical study

2.10.1. Conductivity

The DC electrical conductivity of oligoesters with and without I_2doping was studied from 1 V to 10 V using Keithley Electrometer (6517 B). The oligoesters' conductivity was studied for96hrs with an interval of 24 hrs. The conductivity of oligoesters increases with increase in the contact time. The doping of I_2 with oligoester and its conductivity are affected by the electron density of azine nitrogen in the molecules, as illustrated in SF. 20.

The charge density of azine nitrogen is calculated using DFT study and they vary in the order DMDAP (–0.261) > DMDMP (–0.157) > DMDOP (–0.101)), which is the same as the conductivity of the respective oligoesters. The conductivity of oligoesters were calculated using the formula σ = [(I X L) / (V X A)] [65]. Here, the voltage is V, thickness of the pellet is L, cross–sectional pellet area is A and current is mentioned as I. The conductivity measurements of oligoesters were taken in air atmosphere and the graph was plotted between I_2 contact time vs conductivity. When the I_2 comes into contact with electron donating azine nitrogen produces polarons and I_3^- counter ions in the structure of oligoesters. This is due to the formation of charge transfer complex between dopant I_2 with azine nitrogen and aromatic π carbons of oligoesters [66]. The coordination mode of I_2 with nitrogens and phenyl rings is shown in SF. 21.Polaron formation in the oligoester system improves electron mobility and increases electrical conductivity.

The I_2 doped oligoesters FT–IR and UV–Vis spectra are shown in SF. 22 and 23. The bonds between the atoms in the oligoesters were modified by adding I_2 doping and increasing the polarons(–C = N– to = C–N^+–) in the structure. This polaron is weakening the aromatic –C–H stretching vibration band between 2750 and 2520cm^{-1} confirms the interaction of I_2 with the π e^- system of the oligoesters[67]. Similarly, the appearance of broad bands between 1686 and 1420 cm^{-1}giving the evidence ofinteraction of I_2 with –C = C– and –C = N– groups of oligoesters. These outcomes indicate the incorporation of I_2 in the backbone of the oligoesters chain [68].The contour map of oligoesters in SF. 18 show that there is a weak electron flow between two repeating units due to the ester linkage of oligoesters. Even though, DMDAP dimer structure exhibits high electrical conductivity due to high electron density nitrogen and flexible structure which induces the π–π stacking interaction, revealing high electrical conductivity.

In the UV–Vis spectra of oligoesters, the absorption bands are redshifted and appear at 352, 357 and 371 nm for DMDMP, DMDOP and DMDAP respectively. Tauc method was used to determine the band gap value of oligoesters and are 3.06, 3.12 and 2.93eV for DMDMP, DMDOP and DMDAP respectively. The I_2 doped oligoesters have reduced band gap, which improves electrical conductivity.After 96 hrs of I_2 doping, the conductivity of oligoesters is in the order of DMDAP > DMDMP > DMDOP. The DMDAP has higher electrical conductivity ($10^{-3}Scm^{-1}$) than the other two oligoesters ($10^{-4}Scm^{-1}$) because of having π–π stacking contact between the repeating units and higher charge density on nitrogens [69]. The DC conductivity results confirm that the oligoesters can be used as optoelectronic, semiconducting materials in electronic and photovoltaic applications.

3.1. AC electrical study

3.1.1. Dielectric property

The dielectric constant and dielectric loss of oligoester were evaluated with different frequencies and temperatures. The results are plotted against logarithmic frequency and are shown in SF.24. The dielectric constant value of the oligoester was calculated using the formula $\varepsilon r = Cd/\varepsilon_0 A$ [70]. Here, the crosssectional area is A, capacitance is C, free–space permittivity of the pellet is ε_0 and thickness of

the pellet is d. The dielectric constant values of oligoestersaredecreasing with increase in the frequency and reaches a constant value at a certain point. The oligoesters exhibit high dielectric constant value at lower frequencies and low dielectric constant at higher frequencies. The oligoesters have enough time to align with the field before changing direction at lower frequency. So, oligoesters exhibit higher dielectric constant values at lower frequency.

The dielectric constant value of oligoesters increases when the temperature is increased at a lower frequency due to decrease in the intramolecular force between the oligoesters.

At low temperatures, the segmental motion of the oligoesters chain is frozen and the dielectric constant value is low. The thermal agitation of the oligoester chain increases with increase in temperature and causes high dielectric constant value. The dielectric constant value of the oligoesters at different temperatures is shown in SF. 25. Among the oligoesters, DMDMP has the highest dielectric constant value, while DMDAP has the lowest dielectric constant value at constant frequency.

The dielectric constant of oligoesters is highly related to dipole moment value of the system. The dipole moment dimer of oligoesters' was calculated using DFT in the

B3LYP/6–311 + + G(d,p) level basis set and are found to be 2.1864D, 2.1240D, 1.7388D for DMDMP, DMDOP and DMDAP respectively. The DMDMP has high dielectric constant value at a constant frequency. Because of its large dipole moment and loosely connected π bonds, cause easily polarised and havehigher dielectric constant than the other oligoesters[71].

Thus, the DMDMP can be used to make passive components such as resistors, capacitors etc.,[72]. Since the dielectric loss of oligoesters is high at low frequency and low value at higher frequency ranges, they are suitable for electro–optical device applications[73].

3.1.2. Impedance study

Figure 26 shows the impedance of oligoesters' real (Z') and imaginary (Z") parts at various frequencies and temperatures ranging from 303K to 393K. The oligoesters exhibit a high impedance value at lower temperatures and frequencies of the oligomer system. This is due to the dipolar polarization and orientation of the oligomeric substance. The real portion (Z') of impudence decreases as frequency increases due to increased electron mobility between its monomeric units. At higher frequencies, the Z' value in the oligomer system is practically constant due to the decrease in band gap value caused by increased electron mobility. These results were obtained due to the dissipation of space charges, which promotes electron mobility, lowers the dielectric, and increases conductivity[67].

The imaginary component (Z") of the impedance study decreased with increasing frequency for all temperatures. These figures show an increase caused by oligoester relaxation [68]. After reaching their peak height at the lower frequency level, the height of the Z" peaks begins to decrease as they migrate to the higher frequency side. It suggests that as the temperature rises, so does the length of relaxation. Peak height and oligoester resistance mechanism are connected linearly. The maximum height of the impedance decreases as temperature and frequency rise. It demonstrates how the resistance decreases as the mobility of the polarons rises[69].

Conclusion

Highly selective azine monomer (DBHMD) and three oligoesters (DMDMP, DMDOP and DMDAP) were synthesized by solution polycondensation using three different acid chlorides such asphenyl phosphonic dichloride, phenyl dichlorophosphate and adipoyl chloride technique. The structure of synthesized compounds was confirmed by FT–IR, ^{1}H, ^{13}C and ^{31}P–NMR spectroscopic techniques. GC–MS and GPC analysis were used to study the molecular weight of monomer and oligoesters respectively. TGA analysis, reveals that oligoesters exhibit good extinguishing behaviour. The contact angle measurements of monomer exhibit hydrophilic nature. UV–Vis and fluorescence spectroscopy studies were used to determine the photophysical properties of fluorophores and found oligoesters have higher band gap and fluorescence intensity value than the monomer. Fluorophores exhibit dual emission in the fluorescence spectrum due to keto–enol tautomer formed in the excited state. In the chemosensor study, fluorophores selectively detect Cu^{2+} ions through fluorescence quenching.Interference, pH and time effect studies reveal the sensing capability of fluorophores with Cu^{2+} ion. The binding constants and stoichiometry of fluorophore with Cu^{2+} ion were calculated using the Stern–Volmer and Benesi–Hildebrand plots. In the reversibility study, fluorophores show good recoverability with Cu^{2+} ion upon the addition of EDTA.

The practical applicability of fluorophores towardsthe detection of Cu^{2+} ion was determined with two lake water samples and shows good response and recoverability. The cell image study of DMDMP and DMDMP–$Cu^{2+}$with THP–1revealed the lack permeability into the

cell wall and and absence of expected cell imaging response. Quenching mechanism, DC and AC electrical results are explained with DFT analysis. Thecharge transfer between fluorophores and quencher were analyzed using global descriptor and ECT and found LMCT process in the chemosensor study. Among all oligoesters, DMDAP exhibited high electrical conductivity due to its high charge density on azine nitrogenand highly polarized loosely attached πbonds in oligoester chain. The images' peaks show the relaxing process of the oligomer system, which corresponds to the real (Z') and imaginary part (Z") of the impedance values of oligoesters at room temperature.DMDMP has high dielectric constant value because of its high dipole moment value andpolarized π e– system. Therefore, DMDMP can be used to make passive components such as capacitors and resistors.

Declarations

Author Contribution

Subramani Manigandan- Preparation of ManuscriptAthianna Muthusamy- Main ManuscriptSiddeswaran Anand- Scheme of manuscript All authors reviwed Manuscript

References

1. Chandra R, Ghorai A, Patra GK (2018) A Simple Benzildihydrazone Derived Colorimetric and Fluorescent ‘on–off-on’ Sensor for Sequential Detection of Copper(II) and Cyanide Ions in Aqueous Solution. Sens Actuators B Chem 255:701–711. 10.1016/j.snb.2017.08.067
2. Li P, Duan X, Chen Z, Liu Y, Xie T, Fang L, Li X, Yin M, Tang BA (2011) Near-Infrared Fluorescent Probe for Detecting Copper(II) with High Selectivity and Sensitivity and Its Biological Imaging Applications. Chem Commun 47:7755–7757. 10.1039/c1cc11885d
3. Robinson NJ, Winge DR (2010) Copper Metallochaperones. Annu Rev Biochem 79:537–562
4. Qi X, Jun EJ, Xu L, Kim SJ, Hong JSJ, Yoon YJ, Yoon J (2006) New BODIPY Derivatives as OFF-ON Fluorescent Chemosensor and Fluorescent Chemodosimeter for Cu2+: Cooperative Selectivity Enhancement toward Cu2+. J Org Chem 71:2881–2884. 10.1021/jo052542a
5. Huang X, Miao Q, Wang L, Jiao J, He X, Cheng Y (2013) A Highly Sensitive and Selective Fluorescence Chemosensor for Cu 2 + and Zn2 + Based on Solvent Effect. Chin J Chem 31:195–199. 10.1002/cjoc.201200619
6. Georgopoulos PG, Wang SW, Georgopoulos IG, Yonone-Lioy MJ, Lioy PJ (2006) Assessment of Human Exposure to Copper: A Case Study Using the NHEXAS Database. J Expo Sci Environ Epidemiol 16:397–409. 10.1038/sj.jea.7500462
7. Cowan JA (1997) Inorganic Biochemistry: An Introduction, 2nd Edition. 456
8. Kozlowski H, Luczkowski M, Remelli M, Valensin D (2012) Copper, Zinc and Iron in Neurodegenerative Diseases (Alzheimer’s, Parkinson’s and Prion Diseases). Coord Chem Rev 256:2129–2141
9. Xiong J, Liu X, Cheng QY, Xiao S, Xia LX, Yuan BF, Feng YQ (2017) Heavy Metals Induce Decline of Derivatives of 5-Methycytosine in Both DNA and RNA of Stem Cells. ACS Chem Biol 12:1636–1643. 10.1021/acschembio.7b00170
10. Zhang X, Shiraishi Y, Hirai T (2007) Cu(II)-Selective Green Fluorescence of a Rhodamine-Diacetic Acid Conjugate. Org Lett 9:5039–5042. 10.1021/ol7022714
11. Gaggelli E, Kozlowski H, Valensin D, Valensin G (2006) Copper Homeostasis and Neurodegenerative Disorders (Alzheimer’s, Prion, and Parkinson’s Diseases and Amyotrophic Lateral Sclerosis). Chem Rev 106:1995–2044
12. Gupta VK, Jain AK, Maheshwari G, Lang H, Ishtaiwi Z (2006) Copper(II)-Selective Potentiometric Sensors Based on Porphyrins in PVC Matrix. Sens Actuators B Chem 117:99–106. 10.1016/j.snb.2005.11.003
13. Chen X, Jou MJ, Lee H, Kou S, Lim J, Nam SW, Park S, Kim KM, Yoon J (2009) New Fluorescent and Colorimetric Chemosensors Bearing Rhodamine and Binaphthyl Groups for the Detection of Cu2+. Sens Actuators B Chem 137:597–602. 10.1016/j.snb.2009.02.010
14. Liu H, Cui S, Shi F, Pu S (2019) A Diarylethene Based Multi-Functional Sensor for Fluorescent Detection of Cd2 + and Colorimetric Detection of Cu2+. Dyes Pigm 161:34–43. 10.1016/j.dyepig.2018.09.030
15. Jung JM, Lee SY, Kim C (2017) A Novel Colorimetric Chemosensor for Multiple Target Metal Ions Fe2+, Co2+, and Cu2 + in a near-Perfect Aqueous Solution: Experimental and Theoretical Studies. Sens Actuators B Chem 251:291–301. 10.1016/j.snb.2017.05.055
16. Kim MS, Jung JM, Kang JH, Ahn HM, Kim PG, Kim C (2017) A New Indazole-Based Colorimetric Chemosensor for Sequential Detection of Cu2 + and GSH in Aqueous Solution. Tetrahedron 73:4750–4757. 10.1016/j.tet.2017.06.051

17. Jin X, Wang S, Yin W, Xu T, Jiang Y, Liao Q, Xia X, Liu J (2017) A Highly Sensitive and Selective Fluorescence Chemosensor for Fe3 + Based on Rhodamine and Its Application in Vivo Imaging. Sens Actuators B Chem 247:461–468. 10.1016/j.snb.2017.03.084
18. Ko SK, Chen X, Yoon J, Shin I (2011) Zebrafish as a Good Vertebrate Model for Molecular Imaging Using Fluorescent Probes. Chem Soc Rev 40:2120–2130. 10.1039/c0cs00118j
19. Mukherjee S, Hazra S, Chowdhury S, Sarkar S, Chattopadhyay K, Pramanik A (2018) A Novel Pyrrole Fused Coumarin Based Highly Sensitive and Selective Fluorescence Chemosensor for Detection of Cu2 + Ions and Applications towards Live Cell Imaging. J Photochem Photobiol Chem 364:635–644. 10.1016/j.jphotochem.2018.07.004
20. Yin S, Leen V, Snick S, van Boens N, Dehaen W (2010) A Highly Sensitive, Selective, Colorimetric and near-Infrared Fluorescent Turn-on Chemosensor for Cu2 + Based on BODIPY. Chem Commun 46:6329–6331. 10.1039/c0cc01772h
21. Tharmalingam B, Mathivanan M, Dhamodiran G, Saravana Mani K, Paranjothy M, Murugesapandian B (2019) Star-Shaped ESIPT-Active Mechanoresponsive Luminescent AIEgen and Its On–Off–On Emissive Response to Cu2+/S2−. ACS Omega 4:12459–12469. 10.1021/acsomega.9b00845
22. Hien NK, Bao NC, Ai Nhun NT, Trung NT, Nam PC, Duong T, Kim JS, Quang DT (2015) A Highly Sensitive Fluorescent Chemosensor for Simultaneous Determination of Ag(I), Hg(II), and Cu(II) Ions: Design, Synthesis, Characterization and Application. Dyes Pigm 116:89–96. 10.1016/j.dyepig.2015.01.014
23. Jin X, Gao J, Xie P, Yu M, Wang T, Zhou H, Ma A, Wang Q, Leng X, Zhang X (2018) Dual-Functional Probe Based on Rhodamine for Sequential Cu2 + and ATP Detection in Vivo. Spectrochim Acta Mol Biomol Spectrosc 204:657–664. 10.1016/j.saa.2018.06.094
24. McQuade DT, Hegedus AH, Swager TM (2000) Signal Amplification of a Turn-on Sensor: Harvesting the Light Captured by a Conjugated Polymer. J Am Chem Soc 2000, 122, 12389–12390
25. Karao lu K, Serbest K, Emirik M, Şahin E (2015) An Unsymmetrical Ferrocene Based Azine and Its Cu(II) Complex: Spectroscopy, Crystal Structure, Electrochemistry and DFT Calculations. J Organomet Chem 775:80–87. 10.1016/j.jorganchem.2014.10.021
26. Sheng R, Wang P, Liu W, Wu X, Wu S (2008) A New Colorimetric Chemosensor for Hg2 + Based on Coumarin Azine Derivative. Sens Actuators B Chem 128:507–511. 10.1016/j.snb.2007.07.069
27. Ismet K, Vilayetoglu AR (2002) Synthesis and Characterization of Oligosalicylaldehyde-Graft-Oligoaniline and Its Beginning Oligomers. J Appl Polym Sci2002 85:218–226. 10.1002/app.10623
28. Armarego WLF (1980) Purification of Laboratory Chemicals; 4th ed.; Reed Educational and Professional: Canberra A C T, Australia. ISBN 9780128054574
29. Kolcu F, Kaya İ (2016) Synthesis and Characterization of Conjugated Polyphenols Derived from Azomethine Formation Containing Terephtaldehyde via Oxidative Polycondensation. J Macro Sci Part A 53:438–451. 10.1080/10601325.2016.1176445
30. Dineshkumar S, Muthusamy A, Chandrasekaran J (2017) Temperature and Frequency Dependent Dielectric Properties of Electrically Conducting Oxidatively Synthesized Polyazomethines and Their Structural, Optical, and Thermal Characterizations. J Mol Struct 1128:730–740. 10.1016/j.molstruc.2016.09.051
31. Kaniappan K, Murugavel SC (2009) Photocrosslinkable Phosphorus Containing Homo- and Copolyesters: Synthesis, Characterization, and Photosensitive Properties. J App Poly Sci 111:1606–1314. 10.1002/app
32. Alosmanov RM, Azizov AA, Magerramov AM (2011) NMR Spectroscopic Study of Phosphorus-Containing Polymer Sorbent. Russ J Gen Chem 81:1477–1479. 10.1134/s1070363211070127
33. Bautista Y, Gozalbo A, Mestre S, Sanz V (2017) Thermal Degradation Mechanism of a Thermostable Polyester Stabilized with an Open-Cage Oligomeric Silsesquioxane. Materials. 11, 22(1)-22(13). 10.3390/ma11010022
34. Mallakpour S, Dinari M (2013) Chiral Bio-Nanocomposites Based on Thermally Stable Poly(Amide-Imide) Having Phenylalanine Linkages and Reactive Organoclay Containing Tyrosine Amino Acid. Amino Acids 44:1021–1029. 10.1007/s00726-012-1436-2
35. Wu H, Ortiz R, Correa RDA, Krifa M, Koo JH (2018) Self-Extinguishing and Non-Drip Flame Retardant Polyamide 6 Nanocomposite: Mechanical, Thermal, and Combustion Behavior. Flame Retardancy Therm Stab Mater 1:1–13. 10.1515/flret-2018-0001
36. Caglar A, Cengiz U, Yildirim M, Kaya I (2015) Effect of Deposition Charges on the Wettability Performance of Electrochromic Poly. Appl Surf Sci 331:262–270. 10.1016/j.apsusc.2015.01.103
37. Liang S, Tong Q, Qin X, Liao X, Li Q, Yan G (2020) A Hydrophilic Naphthalimide-Based Fluorescence Chemosensor for Cu2 + Ion: Sensing Properties, Cell Imaging and Molecular Logic Behavior. Spect.chim. Acta. A Mol. Bio Spectr 230:118029. 10.1016/j.saa.2020.118029

38. Anand S, Muthusamy A (2019) Synthesis, Characterization, Electrochemical, Electrical, Thermal and ESIPT Behaviour of Oligobenzimidazoles of Certain Substituted Benzimidazole Carboxylic Acids and Their Diode Applications. J Mol Struct 1177:78–89. 10.1016/j.molstruc.2018.09.045
39. Ikabata Y, Wang Q, Yoshikawa T, Ueda A, Murata T, Kariyazono K, Moriguchi M, Okamoto H, Morita Y, Nakai H (2017) Near-Infrared Absorption of π-Stacking Columns Composed of Trioxotriangulene Neutral Radicals. NPJ Quantum Mater 2:1–6. 10.1038/s41535-017-0033-8
40. Karsten BP, Viani L, Gierschner J, Cornil J, Janssen RAJ (2008) An Oligomer Study on Small Band Gap Polymers. J Phys Chem A 112:10764–10773. 10.1021/jp805817c
41. Dineshkumar S, Muthusamy A (2016) Synthesis and Spectral Characterization of Cross Linked Rigid Structured Schiff Base Polymers: Effect of Substituent Position Changes on Optical, Electrical, and Thermal Properties. Polym Plas Tech Engi 55:368–378. 10.1080/03602559.2015.1098680
42. Oter O, Ertekin K, Kilincarslan R, Ulusoy M, Cetinkaya B (2007) Photocharacterization of a Novel Fluorescent Schiff Base and Investigation of Its Utility as an Optical Fe3 + Sensor in PVC Matrix. Dye Pigm 74:730–735. 10.1016/j.dyepig.2006.05.006
43. Johnson ER, Keinan S, Mori-Sánchez P, Contreras García J, Cohen AJ, Yang W (2010) Revealing Noncovalent Interactions. J Am Chem Soc2010 132:6498–6506. 10.1021/ja100936w
44. Lei YQ, Xi JY, Guo H, Jia R (2018) DFT/TDDFT Methods Analysis of ESIPT Process in a Series of 7-Hydroxy-1-Indanone Derivates and New Dyad Design. J Saudi Chem Soc 22:777–785. 10.1016/J.JSCS.2017.12.009
45. Wang Y, Yang G, Zhang Q, Song X, Yang D (2018) Theoretical Explorations about the Excited State Behaviors for Two Novel High Efficient ESIPT Compounds. Struct Chem 29:1817–1823. 10.1007/s11224-018-1165-6
46. Kuzu B, Tan M, Ekmekci Z, Menges N (2017) A Novel Fluorescent Sensor Based on Imidazole Derivative for Fe3 + Ions. J Lumin 192:1096–1103. 10.1016/j.jlumin.2017.08.057
47. Li ZX, Zhang LF, Zhao WY, Li XY, Guo YK, Yu MM, Liu JX (2011) Fluoranthene-Based Pyridine as Fluorescent Chemosensor for Fe3+. Inorg Chem Commun 14:1656–1658. 10.1016/j.inoche.2011.06.032
48. Valeur B, Leray I (2000) Design Principles of Fluorescent Molecular Sensors for Cation Recognition. Coor.Chem.Rev.2000, 205, 3–40
49. Guo C, Jiang S, Zhu W, Yang X, Pei M, Zhang G (2015) Polythiophene Based Fluorescent Probe for Copper Ions with High Sensitivity. J Appl Polym Sci 132:1–7. 10.1002/app.42440
50. Patil KS, Mahajan PG, Patil SR (2016) Fluorimetric Detection of Sn2 + Ion in Aqueous Medium Using Salicylaldehyde Based Nanoparticles and Application to Natural Samples Analysis. Spectr Act Mol Bio Spec 170:131–137. 10.1016/j.saa.2016.07.020
51. Yang L, Zhu W, Fang M, Zhang Q, Li C (2013) A New Carbazole-Based Schiff-Base as Fluorescent Chemosensor for Selective Detection of Fe3 + and Cu2+. Spectr Act Mol Bio Spect 109:186–192. 10.1016/j.saa.2013.02.043
52. Saha UC, Dhara K, Chattopadhyay B, Mandal SK (2011) A New Half-Condensed Schiff Base Compound: Highly Selective and Sensitive PH-Responsive Fluorescent Sensor. Org Lett 13:9–12
53. Pallbo J, Sparr E, Olsson U (2019) Aggregation Behavior of the Amyloid Model Peptide NACore. Q Rev Biophys 52:1–10. 10.1017/s0033583519000039
54. Hariharan S, Karthikeyan B (2016) Optical and Surface Band Bending Mediated Fluorescence Sensing Properties of MoS2 Quantum Dots. RSC Adv 6:101700–101777. 10.1039/c6ra21157g
55. Methylamino B (2015) Research Article Open Access Synthesis, Characterization, Single Crystal Structural Studies, Antibacterial Activity and DFT Investigations of 2-Chloro-5-Ethoxy-3,6- Bis(Methylamino)-1,4-Benzoquinone. Pharm Anal Acta 6:1–10. 10.4172/21532435.1000418
56. Glossman mitnik D (2013) Computational Study of the Chemical Reactivity Properties of the Rhodamine B Molecule. Procedia Comput Sci 18:816–825. 10.1016/j.procs.2013.05.246
57. Soto-Rojo R, Baldenebro López J, Glossman Mitnik D (2015) Study of Chemical Reactivity in Relation to Experimental Parameters of Efficiency in Coumarin Derivatives for Dye Sensitized Solar Cells Using DFT. Phy Chem Chem Phys 17:14122–14129. 10.1039/c5cp01387a
58. Chattaraj PK, Sarkar U, Roy DR (2006) Electrophilicity Index. Chem Rev.106, 2065. 10.1021/cr040109f
59. Khan E, Shukla A, Jadav N, Telford R, Ayala AP, Tandon P, Vangala VR (2017) Study of Molecular Structure, Chemical Reactivity and H-Bonding Interactions in the Cocrystal of Nitrofurantoin with Urea. New J Chem 41:11069–11078. 10.1039/C7NJ01345K

60. Mortier WJ, Ghosh SK, Shankar S (1986) Electronegativity Equalization Method for the Calculation of Atomic Charges in Molecules. J Am Chem Soc 108:4315–4320
61. Padmanabhan J, Parthasarathi R, Subramanian V, Chattaraj PK (2007) Electrophilicity Based Charge Transfer Descriptor. J Phy Chem A 111:1358–1361. 10.1021/jp0649549
62. Geerlings P, Proft F, De Langenaeker W (2003) Conceptual Density Functional Theory. Chem Rev 103:1793. 10.1021/cr990029p
63. Shyamal M, Mazumdar P, Maity S, Sahoo GP, Salgado Morán G, Misra A (2016) Pyrene Scaffold as Real-Time Fluorescent Turn-on Chemosensor for Selective Detection of Trace-Level Al3 + and Its Aggregation-Induced Emission Enhancement. J Phy Chem A 120:210–220. 10.1021/acs.jpca.5b09107
64. Ma Y, Luo W, Quinn PJ, Liu Z, Hider RC (2004) Design, Synthesis, Physicochemical Properties, and Evaluation of Novel Iron Chelators with Fluorescent Sensors. J Med Chem 47:634, 9–6362
65. Shaktawat V, Jain N, Saxena R, Saxena NS, Sharma K, Sharma TP (2006) Temperature Dependence of Electrical Conduction in Pure and Doped Polypyrrole. Poly Bull 57:535–543. 10.1007/s00289-006-0580-9
66. Dogan F, Temizkan K, Kaya I (2015) A Novel Shape-Controlled Synthesis of Bifunctional Organic Polymeric Nanoparticles. Polymer 70:59–67. 10.1016/j.polymer.2015.06.007
67. Dilek D, Doan F, Bilici A, Kaya I (2011) Oxidative Synthesis of a Novel Polyphenol Having Pendant Schiff Base Group: Synthesis, Characterization, Non-Isothermal Decomposition Kinetics. Thermo chim Acta 518:72–81. 10.1016/j.tca.2011.02.009
68. Bazaka K, Jacob MV (2017) Effects of Iodine Doping on Optoelectronic and Chemical Properties of Polyterpenol Thin Films. Nanomaterials 7:1–16. 10.3390/nano7010011
69. Pérez EM, Martín N (2015) π-π Interactions in Carbon Nanostructures. Chem Soc Rev 44:6425–6433. 10.1039/c5cs00578g
70. Vimalan M, Kumar TR, Tamilselvan S, Sagayaraj P, Mahadevan CK (2010) Growth and Properties of Novel Organic Nonlinear Optical Crystal: L-Alaninium Tartrate (LAT). Physi B Condens Matter 405:3907–3913. 10.1016/j.physb.2010.06.026
71. Xu H, He G, Chen S, Chen S, Qiao R, Luo H, Zhang D (2021) All-Organic Polymer Dielectrics Containing Sulfonyl Dipolar Groups and π−π Stacking Interaction in Side-Chain Architectures. Macro mole 54:8195–8206
72. Wang D, Dang ZM (2018) Processing of Polymeric Dielectrics for High Energy Density Capacitors.Elsevier Inc. ISBN 9780128132159
73. Arjunan S, Bhaskaran A, Kumar RM, Mohan R, Jayavel R (2012) Effect of Iodic Acid Dopant on the Growth and Structural, Optical, and Electrical Properties of l-Arginine Phosphate Single Crystals. Mater. Manu. Proc. 27, 49–52. 10.1080/10426914.2011.551907

Figures

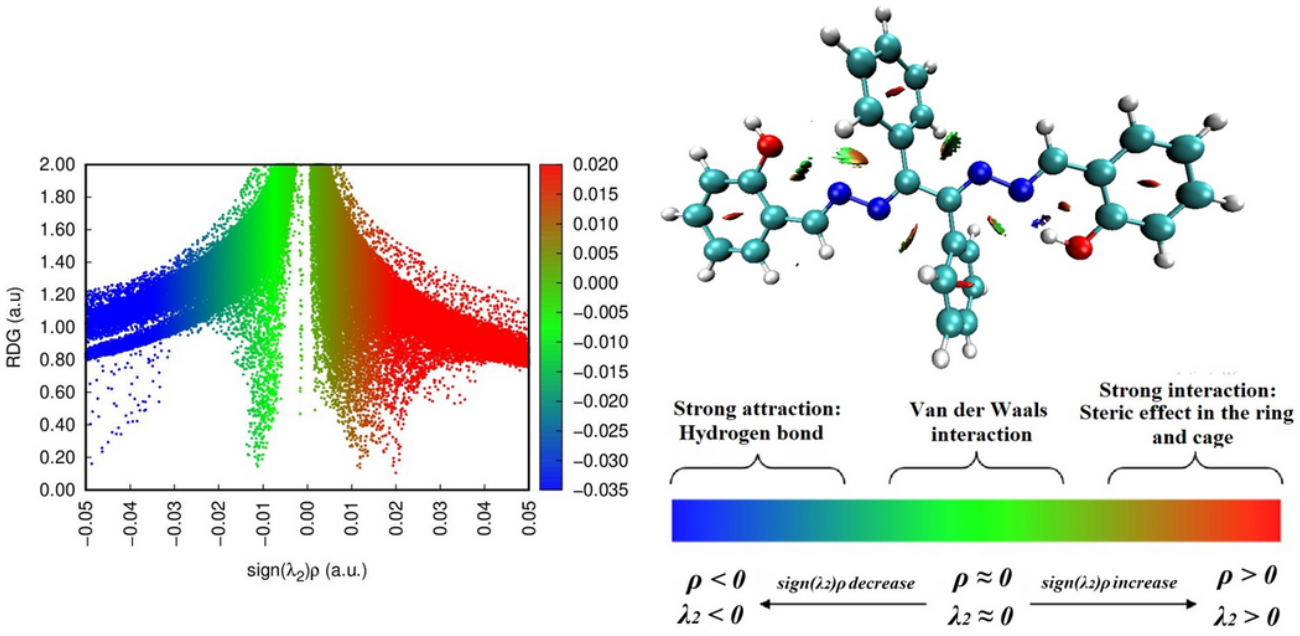

Figure 1

RDG (Y-axis) Vs sign(λ_2)ρ of DBHMD

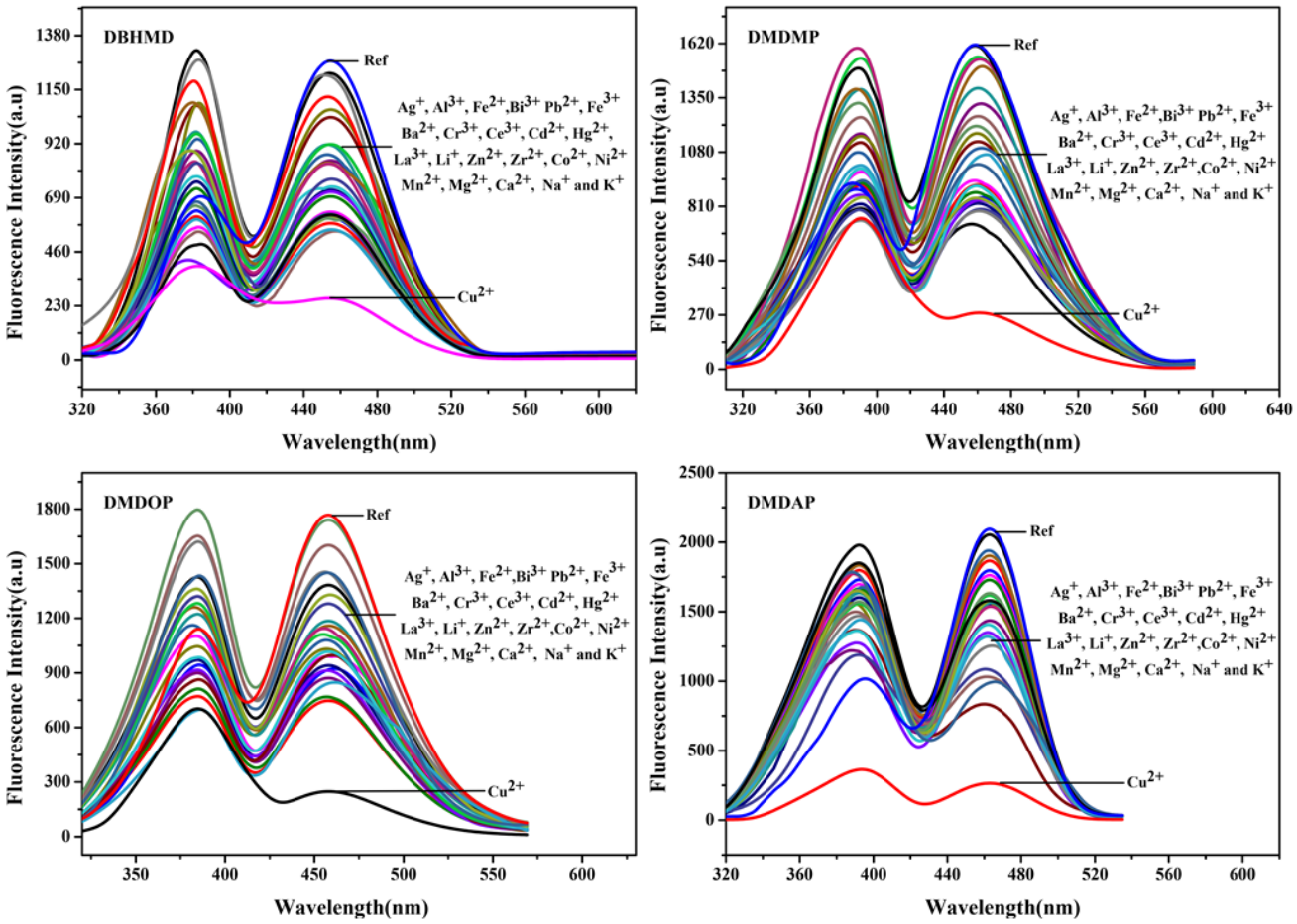

Figure 2

Selective responses of fluorophores with Cu^{2+}in DMF–H_2O solution

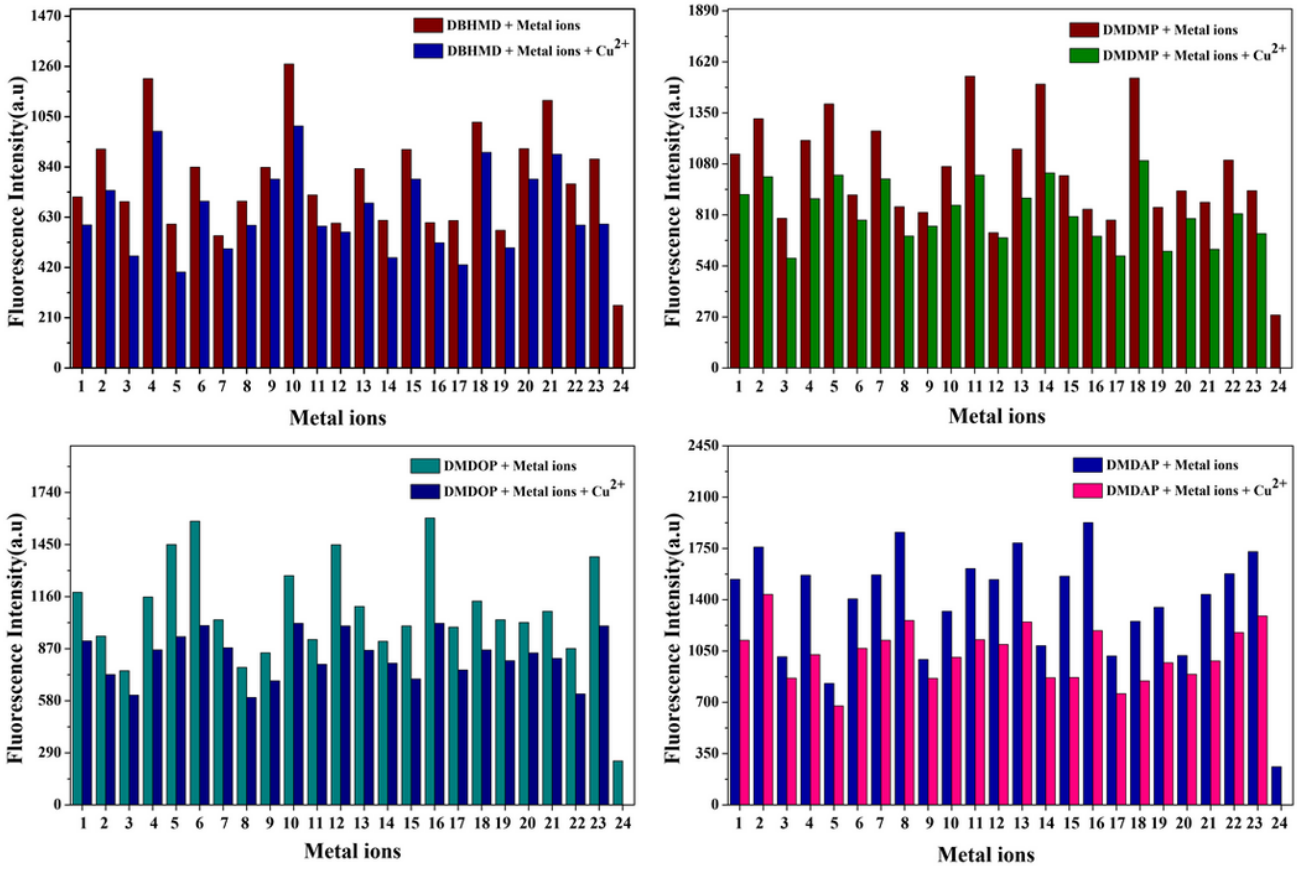

Figure 3

Fluorescence response of fluorophores with Cu^{2+} over the presence of other metal ions (1. Ag^{+}, 2. Al^{3+}, 3. Ba^{2+}, 4. Bi^{3+}, 5. Ca^{2+}, 6. Cd^{2+}, 7. Ce^{3+}, 8. Co^{2+}, 9. Cr^{3+}, 10. Fe^{2+}, 11. Fe^{3+}, 12. Hg^{2+}, 13. K^{+}, 14. La^{+}, 15. Li^{2+}, 16. Mg^{2+}, 17. Mn^{2+}, 18. Na^{+}, 19. Ni^{2+}, 20. Pb^{2+}, 21. Sr^{2+}, 22. Zn^{2+}, 23. Zr^{2+}, 24. Cu^{2+})

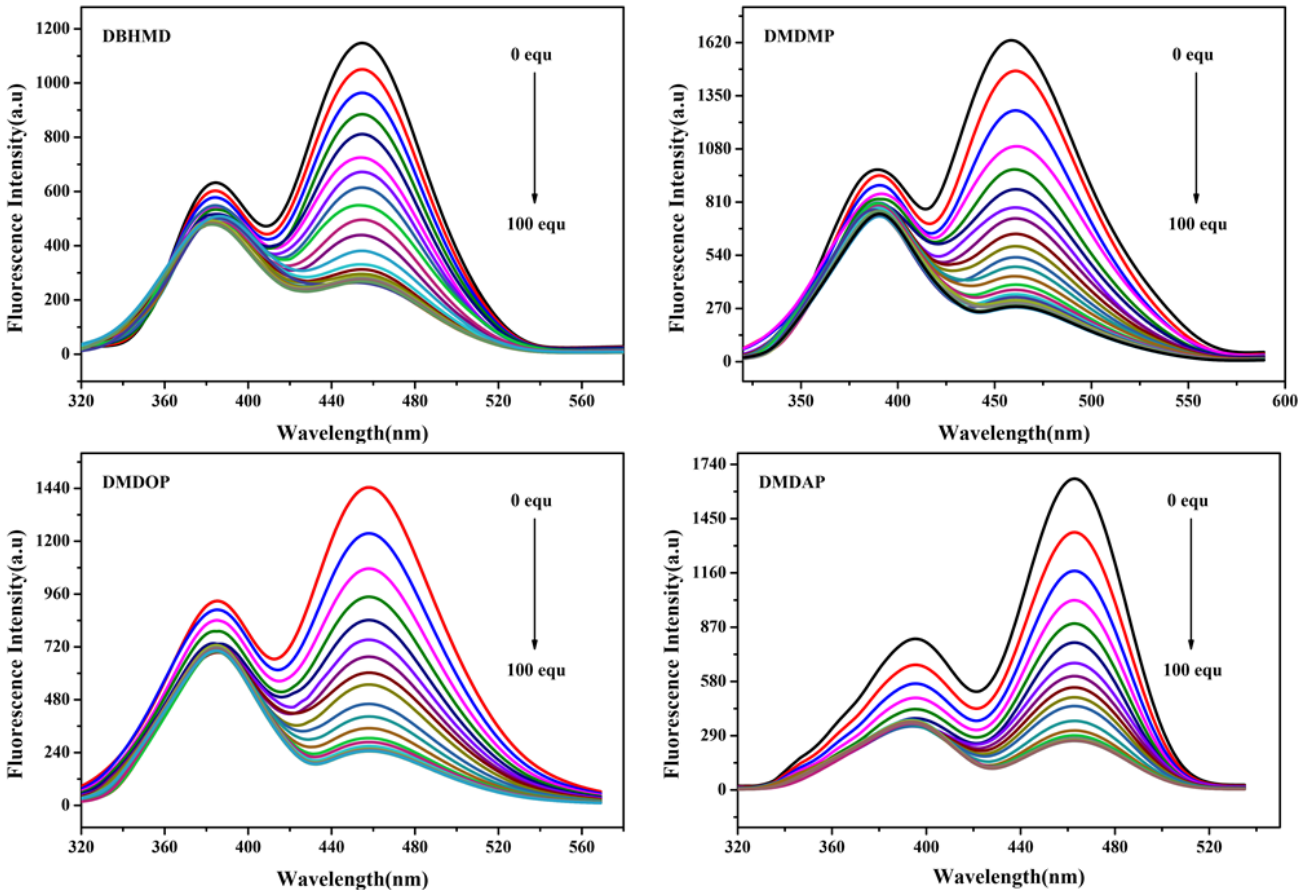

Figure 4

Fluorescence titration of the fluorophore with 0–100 equivalent of Cu^{2+}ion

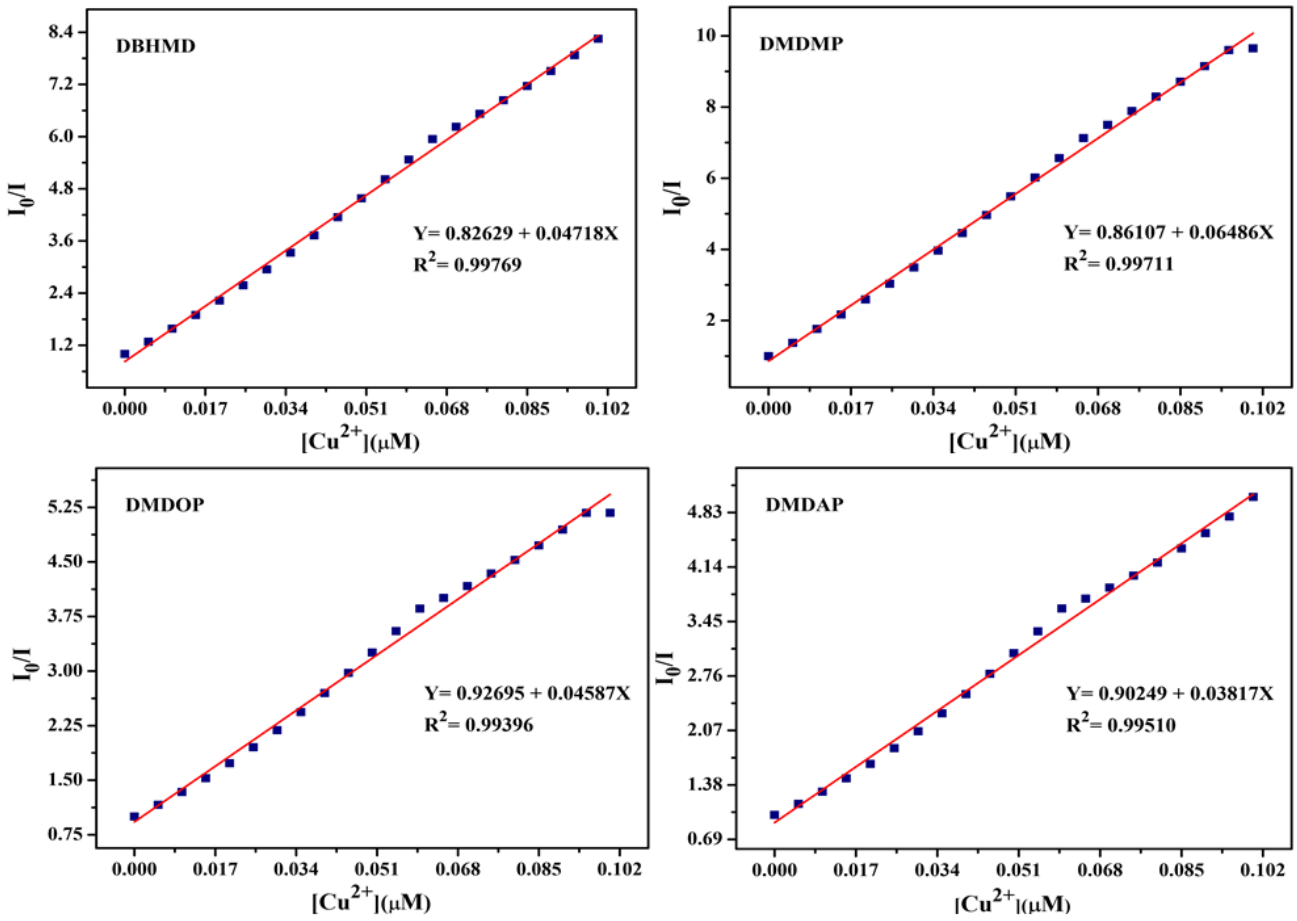

Figure 5

Stern–Volmer plots of monomer and oligoesters

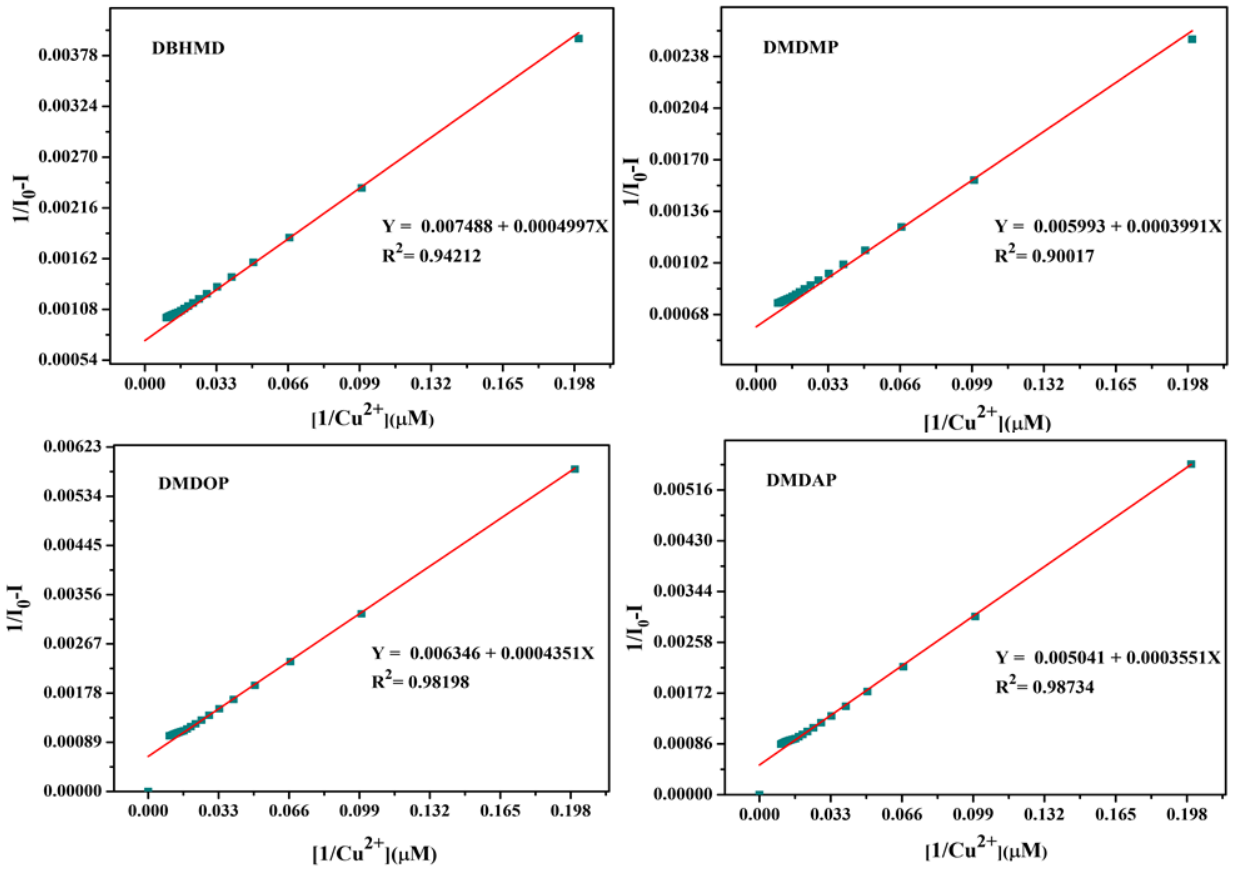

Figure 6

Benesi–Hildebrand binding stoichiometry plots of monomer and oligoesters

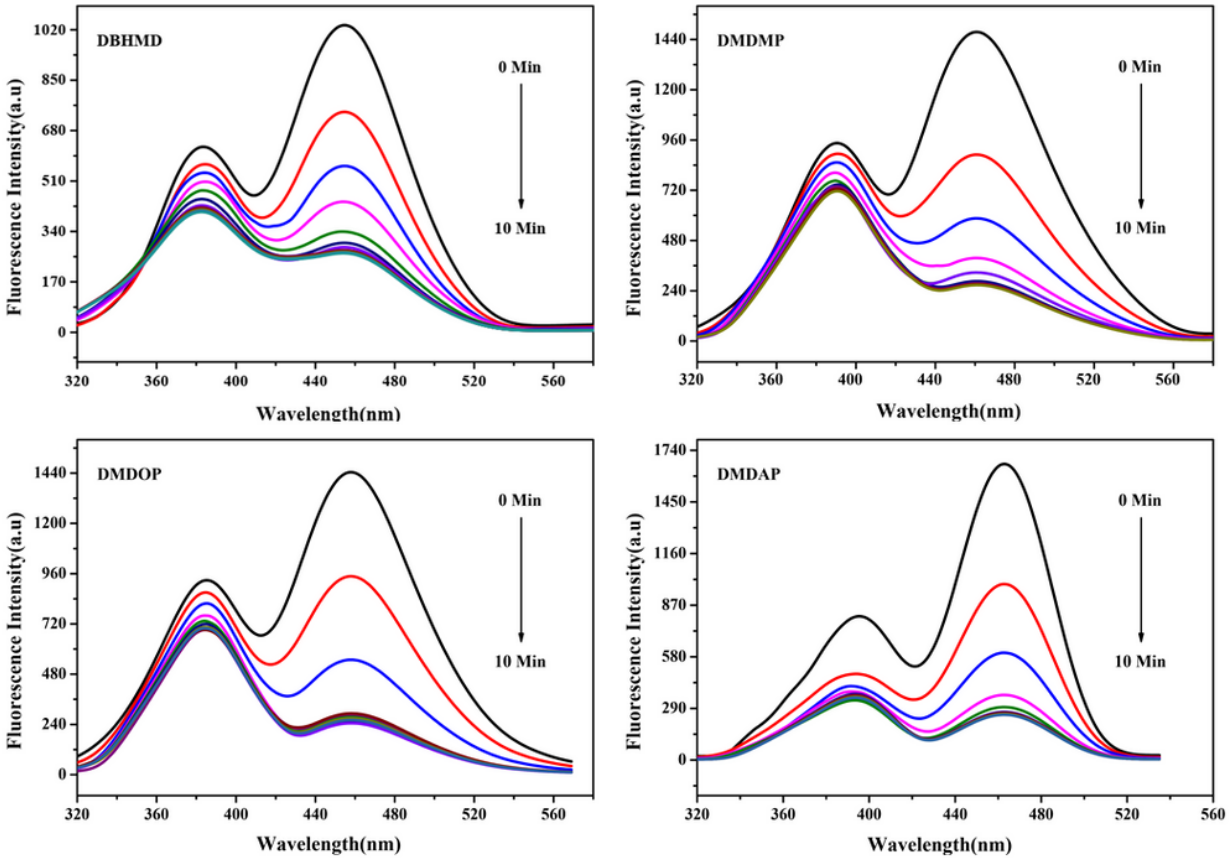

Figure 7

Effect of time on monomer and oligoesters with Cu^{2+} ion

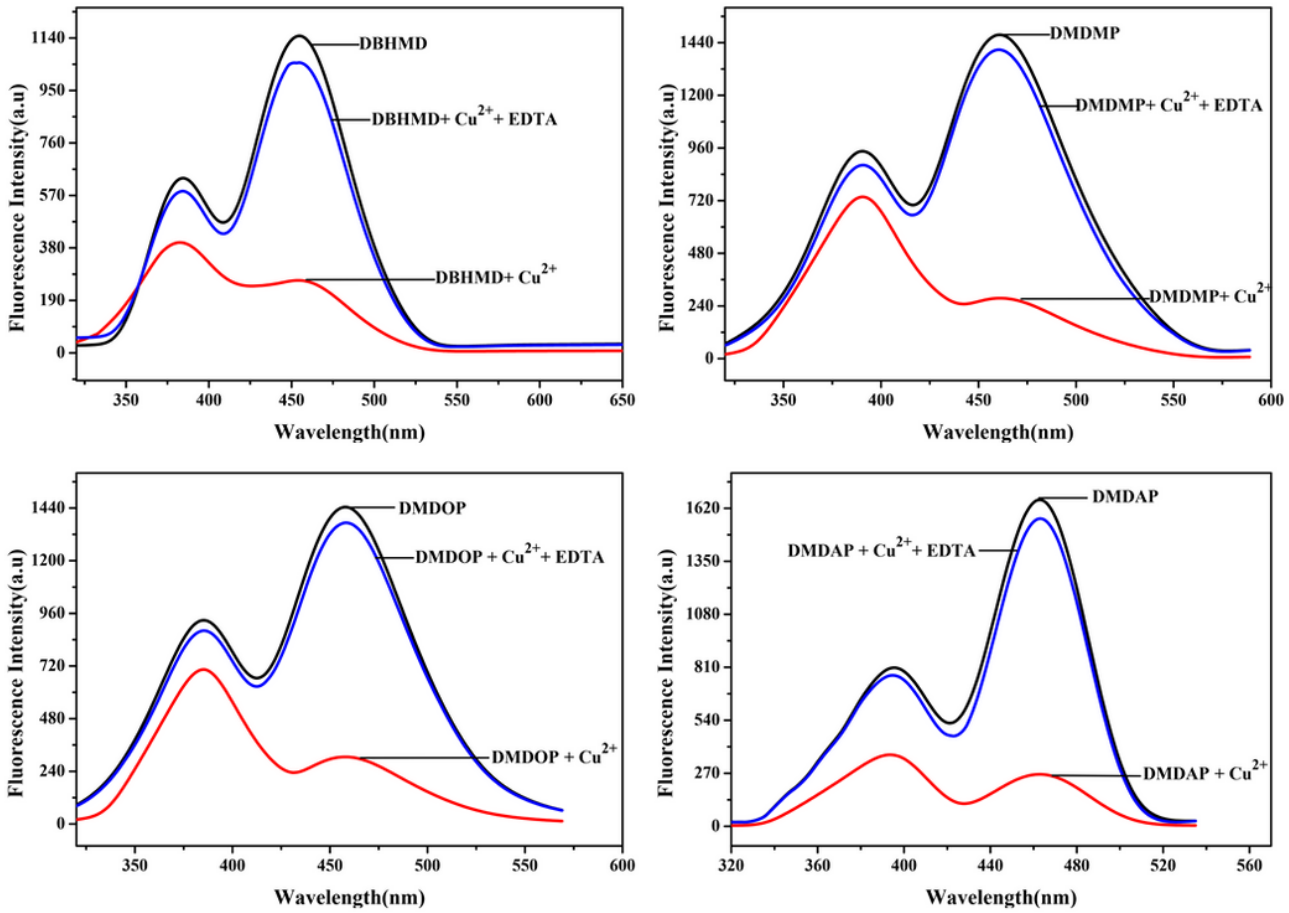

Figure 8

Reversible capability of monomer and oligoesters with EDTA

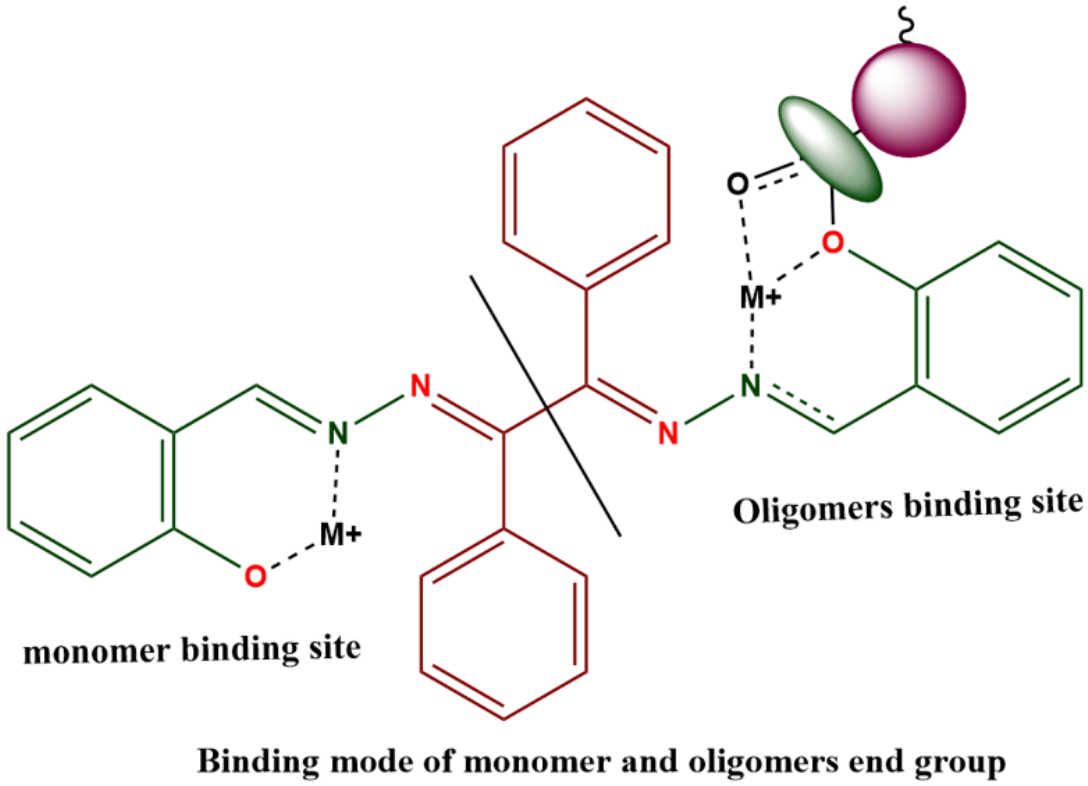

Figure 9

Proposed possible binding mode of azine with Cu^{2+} ion

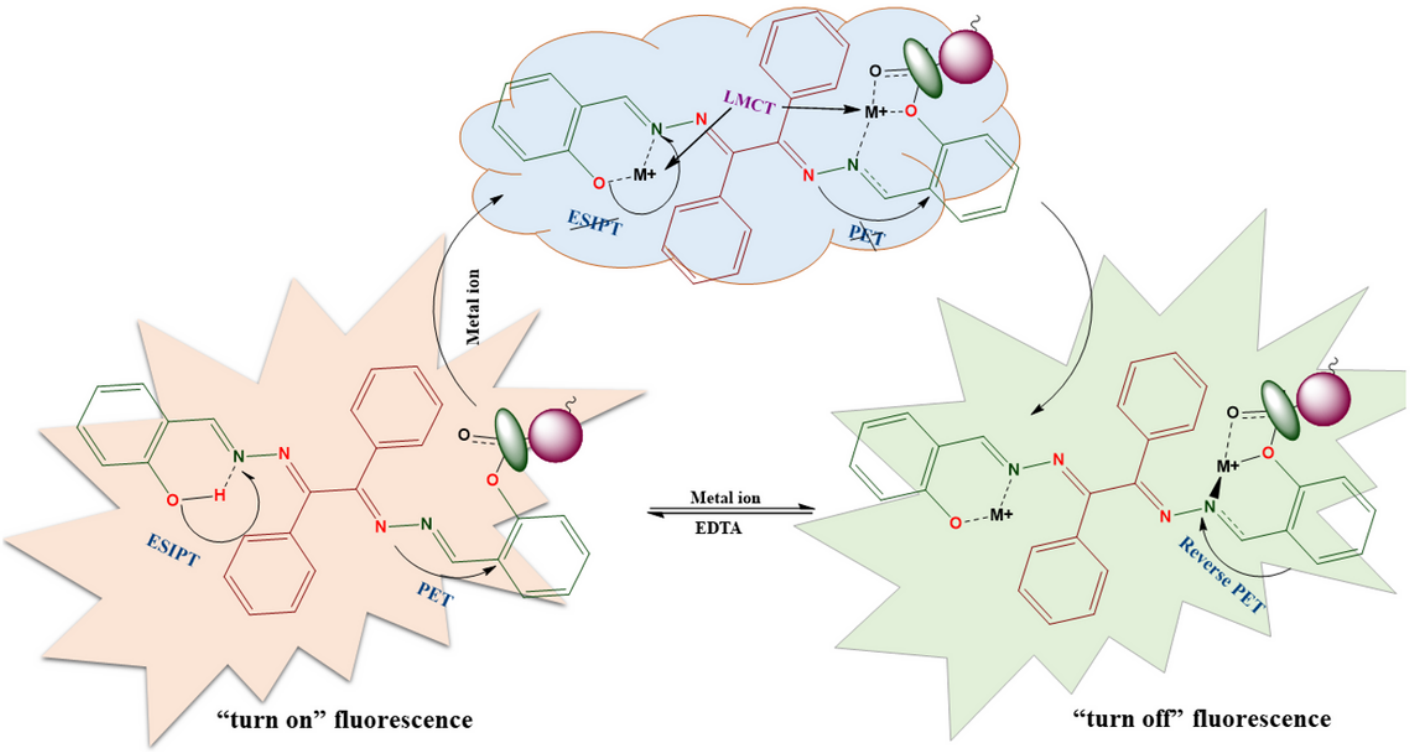

Figure 10

Mechanism of ‘turn off’ fluorescence with Cu^{2+}

Supplementary Files

This is a list of supplementary files associated with this preprint. Click to download.

- SublimentaryfilesPartF.docx